XAFS, IR, and UV−vis study of the Cu-I environment in Cu-I-ZSM-5

ARTICLE *in* THE JOURNAL OF PHYSICAL CHEMISTRY B · JANUARY 1997

Impact Factor: 3.3 · DOI: 10.1021/jp9601577

XAFS, IR, and UV−Vis Study of the Cu^I Environment in Cu^I-ZSM-5

C. Lamberti, S. Bordiga, M. Salvalaggio, G. Spoto, and A. Zecchina*

Dipartimento di Chimica Inorganica, Chimica Fisica e Chimica dei Materiali, Università di Torino, I-10125 Via P. Giuria 7, Torino, Italy

F. Geobaldo

Dipartimento di Scienza dei Materiali e Ingegneria Chimica, Politecnico di Torino, Corso Duca degli Abruzzi 24, I-10129 Torino, Italy

G. Vlaic

Dipartimento di Scienze Chimiche, Via Valerio 28, Trieste, and Sincrotrone Trieste SCpA, Padriciano 99, I-34012 Trieste, Italy

M. Bellatreccia

Dipartimento di Chimica, Universitá "La Sapienza", Piazzale Aldo Moro 5, I-00185 Roma, Italy

Received: January 12, 1996; In Final Form: October 14, 1996[⊗]

XAFS, IR, and UV−vis (diffuse reflectance and photoluminescence) spectroscopies have been employed to investigate the local environment of Cu^I in Cu^I-ZSM-5 prepared by gas phase reaction of H-ZSM-5 (SiO_2/Al_2O_3 = 90−50) with CuCl. The measurements confirm that the absolutely predominant copper species formed with this procedure are Cu^I:Cu species in other oxidation states are less than 1%. Direct proof of the absence of both unreacted CuCl microaggregates and of copper clusters in the zeolite channels is also given. Cu^I-ZSM-5 prepared in this way represents a model solid for investigating the structure of isolated Cu^I sites in zeolites. EXAFS analysis reveal that, *in vacuum* conditions, Cu^+ cations are surrounded by 2.5 ± 0.3 oxygens at 2.00 ± 0.02 Å. The combined use of EXAFS, IR, and photoluminescence UV−vis spectroscopies and computer graphic simulations allows to infer that Cu^+ ions in Cu^I-ZSM-5 are located in two families of sites, indicated as **I** and **II**, (site **II** having the highest coordinative unsaturation) which are nearly equipopulated at *RT*. The formation of $Cu^+-(CO)_n$ (n = 1, 2) adducts at *RT* is observed by IR and supported by XAFS spectroscopies. At ≃ 110−120 K, the Cu^I of family **II** adsorbs up to three CO molecules with formation of $Cu^I-(CO)_3$ *cis*-carbonyl complexes; copper(I) in sites **I** are less unsaturated and can form only *cis*-$Cu^I-(CO)_2$. Both sites form, at ≃ 110−120 K, stable *cis*-$Cu^I-(NO)_2$ species. IR spectroscopy gives evidence of the N_2 interaction with both families of sites at ≃ 110−120 K: the formation of stable $Cu^I(N_2)$ adducts even at *RT*.

1 Introduction

The production of undesired NO gas as a coproduct of several industrial and civil reactions being a great problem for modern society, copper-exchanged zeolites have recently attracted great interest as catalysts for the direct conversion of NO into N_2 and O_2.[1] Among them, Cu-ZSM-5 shows the highest activity. Although full conversion conditions are not easily obtained in practical applications, the decomposition reaction over Cu-ZSM-5 is intrinsically stoichiometric, preventing the formation of undesirable N_2O side product.[2] Moreover, Cu-ZSM-5 is not poisoned by O_2, and reducing agents are not required to sustain the catalytic activity.[1,2] The importance and the actuality of the argument is still evident by considering the high number of papers recently published on the topic; see, *e.g.*, refs 3−15.

Due to the fact that excessively exchanged Cu-zeolites are more active in the NO decomposition (see, *e.g.*, the recent review of Kharas *et al.*[14]), most of the data reported up to now refer to more than 100% copper-exchanged samples, which contain mixtures of copper ions in different aggregation and oxidation states. As an example of contributions reporting the copresence of copper species in different oxidation states, we mention the recent work of Kuroda *et al.*[15] and the papers of Tanabe and Matsumoto.[16] The coexistence of different oxidation and aggregation states is proposed also in the work of Iwamoto *et al.*[17] where the investigated zeolite was a ZSM-5 116% exchanged. After thermal treatment *in vacuo*, the latter authors observed Cu^{II}, Cu^I, and unknown Cu species in a percentage of 50%, 40%, and 10%, respectively. Clear evidence for two types of copper species in a number of overexchanged Cu-ZSM-5 catalysts prepared in different ways was also found by Grünert *et al.*[18] Their results obtained by means of a combination of EPR and EXAFS spectroscopies indicate the presence of isolated copper ions as well as small copper particles. The problem related to the presence of different copper species was also investigated by Hamada *et al.* on a ion-exchanged Cu-ZSM-5 catalyst.[19] They compared the EXAFS spectra obtained from a number of copper-based model compounds with those obtained from the catalyst.

From these considerations, it is evident that, for most of the presented cases, the coexistence of different oxidation states and of isolated and clustered copper species cannot be avoided and a structural model for Cu ions consequently cannot be

* Author to whom correspondence should be addressed. Tel, +3911-6707537; Fax, +3911-6707855; E-mail, ZECCHINA@SILVER.CH.UNITO.IT.

⊗ Abstract published in *Advance ACS Abstracts,* December 1, 1996.

S1089-5647(96)00157-5 CCC: $14.00

confidently assessed. This makes the elucidation of structural and catalytic properties of isolated and clustered species, which is of paramount importance in the design of an efficient catalyst, a difficult subject. This fact has strongly suggested that the synthesis and the characterization of a pure copper-ZSM-5 model solid containing only one oxidation state of isolated copper could be a great help in the understanding of the structure of copper ions in zeolites and their role as catalytic centers.

In order to avoid the presence of Cu ions in different oxidation states, a different synthesis route has been undertaken.[20,21] Following this path, a pure Cu^I-ZSM-5 sample has been quantitatively prepared through gas phase reaction of H-ZSM-5 with CuCl at 573 K.[20,21] When pure Cu^I-ZSM-5 is needed as a model solid, this method is preferable to the standard ion exchange procedures using aqueous solutions of divalent copper salts.

In previous contributions, it has been shown that the Cu^I ion readily adsorbs NO at *RT* to give dinitrosylic species which are then (at least partially) transformed into $Cu^{II}(NO)(NO_2)^-$ during the subsequent spontaneous decomposition reaction.[20−22] On this basis, it has been hypothesized that isolated Cu^I can be the precursor of the catalytic active centers for NO decomposition.[20,21] With respect to the past investigation,[4,20,21] the here-adopted sample preparation procedure has been improved, mainly in two important points: (i) a higher quality H-ZSM-5 sample not containing appreciable concentration of Al extraframework species was used in the preparation; (ii) after reaction with CuCl, a longer outgassing step has been adopted, in order to allow the total elimination of unreacted CuCl molecules or $(CuCl)_n$ microparticles trapped in the channels. In the present contribution, using the atomic selectivity of XAFS spectroscopy[23] combined with the IR and UV−vis spectroscopies, we also give direct information on the oxidation and on the coordination state of Cu^I in vacuum conditions and we give proofs of the nearly total absence of both Cu^0 and CuCl clusters in Cu^I-ZSM-5 prepared through a gas phase reaction with CuCl described in refs 20 and 21; EPR and measurements on the catalyst before and after contact with NO allows quantitative results that undesired Cu^{II} species in the virgin sample are less than 0.9% of the total Cu^{II} sites of the catalyst. Unlike previous reports, different samples characterized by SiO_2/Al_2O_3 ratios in the 90−50 interval have been investigated.

The effect of CO dosage on the XAFS spectra are also compared with the results of a parallel investigation by means of IR spectroscopy. The comparison of the results obtained with all the techniques strengthens the conclusion that the copper Cu^I ions are isolated and located in few, structurally well-defined, sites which are easily accessible to ligand molecules and that the most coordinatively unsaturated Cu^I ions show the highest reactivity.

2 Experimental Methods

2.1 Materials. Low aluminium content H-ZSM-5 samples (SiO_2/Al_2O_3 =90−50) characterized by an high external surface area (70 $m^2\ g^{-1}$) kindly supplied by ENICHEM SpA, Centro Ricerche Novara, have been used. The very high crystalline quality of the H-ZSM-5 has been checked through conventional X-ray powder diffraction and through high-resolution electron microscopy. Cu^I-ZSM-5 has been obtained by a reaction with gaseous CuCl at 573 K as detailed in refs 4, 20, and 21.

Following the widely adopted nomenclature introduced by Iwamoto *et al.*,[17] a 100%-exchanged sample contains one Cu atom for every two Al atoms. Consequently, our exchange procedure allows, in principle, obtaining 200%-exchanged samples. That a ≃200% exchange percentage (corresponding, in this ZSM-5, to one Cu^+ ion for every Al framework atom) has been really reached is documented in Figure 1, where the IR spectra in the OH stretching region of the zeolite before and after the ion exchange are reported. In fact, while the absorption spectrum of H-ZSM-5 in the 3800−3400 cm^{-1} spectral range (see curve 1) is characterized by a sharp and intense band at 3750 cm^{-1} due to external silanols and by a broader absorption band centered at 3611 cm^{-1} due to internal-bridged −Si−(OH)−Al− groups,[24] in the Cu^I-exchanged sample (see curve 2) the band of the bridged Brønsted sites is totally absent. On the contrary, the silanol band at 3750 cm^{-1} is nearly unaffected by the ion exchange; thus confirming that the external −Si−OH groups are practically unaffected by CuCl dosage. This behavior is in agreement with the acidity strength of the two sites, which has been demonstrated (by interaction with CO at 77 K) to be considerably higher for the bridged −Si−(OH)−Al− groups.[24] We emphasize that the exchange level of our samples is the highest so far obtained (to our knowledge). Moreover, the absence in Figure 1 of a band at 3660 cm^{-1} due to internal OH groups located on defective Al^{3+} species[21,24] confirms the high crystalline quality of the investigated samples. The information extracted from the IR spectra reported in Figure 1 is of fundamental importance, because it ensures that the XAFS signal is generated by copper species located only in internal −Si−(OCu)−Al− bridged positions, so emphasizing the model nature of the investigated sample. The 200% exchange percentage has also been qualitatively confirmed by the measured μx values before and after the Cu K edge in the x-ray absorption spectra. Finally, let us remark that the collection of Cu K edge EXAFS data from systems where the dilution of copper species is so high (≃1% in weight) is certainly not easy; however, the use of ZSM-5 with lower Si/Al ratios has been discarded in order to minimize the risk of creating nonisolated Cu species and to ensure the model character of the preparation procedure.

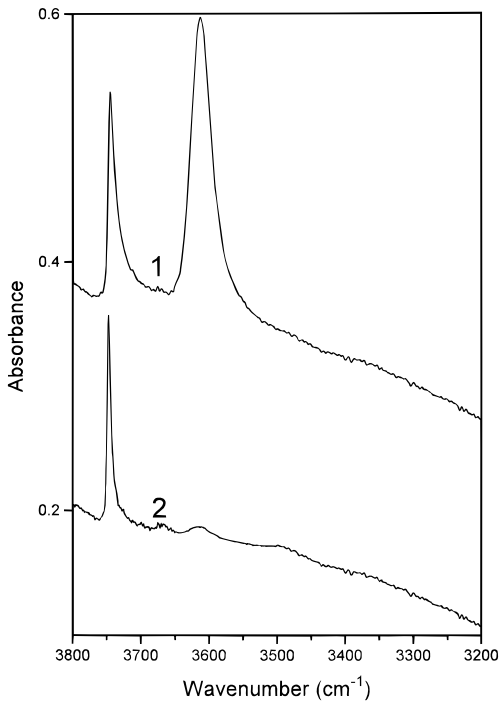

Figure 1. IR spectra of the OH stretching modes of zeolite before (spectrum 1) and after (spectrum 2) the exchange procedure. In spectrum 1, the lack of any relevant absorption around 3660 cm^{-1} assures that extraframework Al^{3+} species are absent, so confirming the high crystalline quality of the investigated sample. In spectrum 2, the total erosion of the 3611 cm^{-1} band indicates that Cu^I cations have substituted nearly all the protons of the internal-bridged −Si−(OH)−Al− sites.

2.2 Characterization Techniques. As the environment of Cu^I is influenced by the presence of adsorbates, XAFS spectroscopy has been performed by using a quartz cell specifically designed to allow measurements under a carefully controlled atmosphere where the sample can be introduced in form of thin self-supporting wafers. This cell, equipped with two Mylar windows, can be connected to (i) a vacuum line for sample pretreatment (degassing for 1 h at 773 K under a dynamic vacuum of *ca.* 10^{-2} Pa); (ii) gas sources, thus allowing the modification of the Cu environment by interaction with well-known amounts of desired adsorbates. All Cu-zeolite samples have been activated under dynamic vacuum at 673 K for 2 h. This cell has already been successfully employed in similar experiments performed on Ti-silicalite[25,26] and Fe-silicalite.[27,28]

We have performed Cu K edge X-ray absorption measurements using the synchrotron radiation emitted by the bending magnet of the EXAFS1 station[29] of LURE (Orsay, France)[30] equipped with a Si(331) channel-cut monchromator (vertical slits width of 0.9 mm). This monchromator, operating with 1 mm vertical slits, has an energy resolution at 10 keV of 1.7 eV[29] (at 9 keV and with a smaller slits overture, a slightly better energy resolution was thus achieved). A Cu metal foil has been used for the angle/energy calibration. The DCI positron storage ring was operating at 1.85 GeV with a current ranging from 315 to 250 mA. XAFS measurements were made at 300 K in transmission mode, at the Cu K edge over a range of 900 eV, with an experimental sampling step of 2 eV (EXAFS), and over a range of 100 eV, with an experimental sampling step of 0.5 eV (XANES); in both cases an integration time of 2.0 s per point has been adopted. Both incident and transmitted photon fluxes have been measured using air-filled ionization chambers. XAFS measurements were performed on Cu-ZSM-5 samples *in vacuo* and in the presence of CO and N_2 adsorbates. Each EXAFS spectrum was recorded at least three times, while only one XANES spectrum has been collected for each experimental condition. Samples homogeneity was controlled by radiographic methods.

Extracted $\chi(k)$ data have been averaged before the EXAFS data analysis. Standard deviation calculated from the averaged spectra was used as an estimate of the statistical noise for the evaluation of the error associated with each structural parameter. The EXAFS data analysis has been performed following standard procedures.[31] Experimental $\chi(k)$ data were extracted from absorption data by a conventional procedure outlined as follows: a linear background was fitted in the pre-edge region, extrapolated to higher energies, and then subtracted from absorption data. Atomic-like contribution was estimated by a polynomial fit and then subtracted from experimental data following the procedure proposed by Lengeler and Eisenberger[32] (more details on the $\chi(k)$ extraction are reported in section 3.1.2). The result was normalized to edge height to obtain experimental $\chi(k)$. The k^3-weighted $\chi(k)$ data were Fourier transformed over a Kaiser window, with $\tau = 2.5$, in the range of 30−800 eV above the edge. Main contributions to the Fourier transform modulus were filtered in order to obtain Cu-nearest-neighbor shell. The so obtained filtered contributions were analyzed using the programs developed by Michalowicz[33] whose nonlinear least-squares fit routines exploit the minimization capabilities of the MINUIT program.[34] The EXAFS results have been obtained by extracting the experimental phase shift and amplitude functions from the model compound Cu_2O. Other details of the procedure followed for the data analysis are described elsewhere.[35] The statistical significance of the results obtained was checked by applying the test proposed by Joyner *et al.*[36]

For IR measurements, thin self-supporting wafers of each zeolite were prepared and activated under dynamic vacuum at 673 K for 2 h inside an IR cell designed to allow *in situ* high-temperature treatments, gas dosage, and low-temperature measurements. The IR spectra were recorded at 2 cm^{-1} resolution on a BRUKER FTIR-66 spectrometer equipped with an mercury cadmium telluride (MCT) cryodetector. For all samples, the spectrum before the gas dosage (CO, N_2, and NO) was used as background and all the IR spectra here reported, except those shown in Figure 1, are background subtracted. Concerning low-temperature spectra, although the IR cell was permanently cooled with liquid nitrogen, the actual sample temperature (under the IR beam) was likely to be *ca.* 110−120 K.

In the UV−vis region, the spectra reported in the literature are mainly given in wavenumbers (cm^{-1}) for absorption data collected in the diffuse reflectance geometry and in wavelength (nm) for emission data. For sake of homogeneity all UV−vis figures will be reported in wavenumbers; however, for sake of clarity, in the discussion all bands will be given in both units. UV−vis diffuse reflectance experiments have been performed with a Varian CARY5 spectrophotometer. Photoluminescence spectra have been recorded on a SPEX Fluorolog-2 spectrofluorometer equipped with a xenon UV−vis−near-IR excitation lamp, whose light is filtered before reaching the sample by an excitation monochromator; the photoluminescence emission is then selected by a second monochromator (emission monochromator) before reaching the photomoltiplier. This photoluminescence apparatus thus allows one to perform both emission and excitation scans, the former by fixing the excitation and scanning the emission monochromator and the latter by fixing the emission and scanning the excitation monochromator. Both monochromators allow a sampling step up to 1 nm in the 200−1000 nm (50000−10000 cm^{-1}) spectral range. All the reported spectra have been collected with an integration time of 1.0 s per point and a sampling step of $\Delta\lambda = 1.0$ nm, which means $\Delta\tilde{\nu} = 250$ cm^{-1} at 200 nm (50000 cm^{-1}) and $\Delta\tilde{\nu}$ 10 cm^{-1} at 1000 nm (10 000 cm^{-1}). Both diffuse reflectance spectroscopy (DRS) and photoluminescence experimental setup allows measurement of the samples under controlled atmospheres.

EPR spectra have been measured at room temperature on a Bruker 300E equipped with an automatic routine for spectra double integration and quantitative calibration.

Computer graphic simulations and modeling of the zeolite framework have been performed using software programs developed by Biosym Technology Inc.,[37] running on a SGI4D35 workstation.

3 Results and Discussion

3.1 X-ray Absorption Spectroscopies. Due to their atomic selectivity and its sensitivity to the local environment of the selected atomic species,[23] several groups attempted to characterize the oxidation and aggregation states of the copper species present in zeolite samples by using EXAFS and XANES techniques before and after thermal treatments in vacuum: see *e.g.* refs 14, 18, 19, and 38−41 for Cu-ZSM-5, refs 15 and 41−44 for Cu-mordenite, refs 16, 41, and 45 for Cu-faujasites, and ref 46 for hydrated Cu-chabazite. In all cases, samples were obtained by means of conventional ion exchange procedures.

XANES and EXAFS data discussed in the following two sections have partially been presented at the XAFS IX conference.[47]

3.1.1 XANES Region. Figure 2 shows the XANES region of the absorption spectra of the Cu-ZSM-5 sample *in vacuo* and

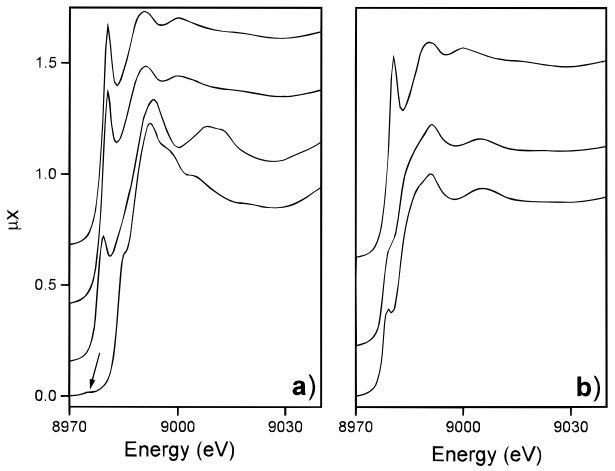

Figure 2. XANES spectra: pre- and near-edge region. (a) (from top to bottom) Cu^I-ZSM-5 *in vacuo*; Cu^I-ZSM-5 after interaction with N_2 (equilibrium pressure of about 300 Torr); Cu_2O and $CuCl_2$ model compounds (reported for the sake of comparison; spectra of CuCl and CuO are omitted for brevity). The arrow in the $CuCl_2$ spectrum evidences the weak absorption attributed to the dipole-forbidden 1s → 3d electronic transition[18,15,51,55] of Cu^{2+} species. (b) (from top to bottom) Cu^I-ZSM-5 *in vacuo*; Cu^I-ZSM-5 after a first dose of CO (equilibrium pressure ≃1 Torr); Cu^I-ZSM-5 after a second dose of CO (equilibrium pressure ≃100 Torr). 1 Torr ≃ 133.3 Pa.

after interaction with N_2 and CO. Absorption spectra of reference compounds Cu_2O and $CuCl_2$ have also been reported in Figure 2a, in order to enable a direct comparison with well-defined Cu^I (d^{10} configuration) and Cu^{II} (d^9 configuration) species.

The pre-edge region of X-ray absorption spectra can give direct information on the oxidation state of copper.[14,48−52] In fact, it is widely recognized that a single well-defined peak at 8983−8984 eV is the fingerprint of copper species in the oxidation state one. This peak is due to the dipole-allowed 1s → 4p electronic transition of Cu^I.[14,15,18,48,51,53,54] On the contrary, Cu^{II} species exhibit: (i) a weak absorption at about 8976−8979 eV, attributed to the dipole-forbidden 1s → 3d electronic transition;[14,15,18,48,51,55] (ii) a shoulder at about 8985−8988 eV and an intense peak at about 8995−8998 eV, both due to 1s → 4p transition.[14,15,48,51,56] All these features are evident in the reference spectra of Cu_2O and $CuCl_2$ reported in Figure 2a.

Because of the great differences between the pre-edge spectra of Cu^I and Cu^{II} ions, XANES spectroscopy has often been used to distinguish, even if in a qualitative way, among the different oxidation states of copper species in zeolites. As an example, the presence of Cu^{II} ions is reported in the results of Hamada *et al.*[19] on Cu^{II}-exchanged ZSM-5 and in those of Choi *et al.*[44] on Cu^{II}-mordenite. Liu and Robota[38] have also reported interesting XANES spectra of Cu-ZSM-5 collected at high temperature in an *ad hoc* reactor located in the X-ray beam line. Kuroda *et al.*[15] have studied the pre-edge region of different Cu-mordenite samples obtained by ion exchanges with aqueous Cu^{2+} solution as a function of the activation temperature from 300 to 873 K (see Figure 7 of ref 15). Samples activated at low temperatures (300, 373, 473, and 573 K) clearly show the predominant presence of Cu^{II} species, while in samples treated at higher temperatures (673, 773, and 873 K) the copresence of Cu^I species is evidentiated. The XANES spectrum of their sample activated at 873 K and containing nearly only Cu^I species is fully comparable with that obtained on our model solid.

Although the presence of a sharp peak at 8982 eV in the XANES spectrum of Cu^I-ZSM-5 outgassed *in vacuo* is indicative of a high concentration of Cu^I ions, the absence of any absorption at 8976 eV (clearly visible in the spectrum of $CuCl_2$; see the arrow in Figure 2a) does not exclude the presence of a minor fraction of Cu^{2+} cations (because its characteristic peak at 8976 eV is intrinsically weak and is certainly overshadowed by the more intense 8982 eV signal generated by the more abundant Cu^+ species). This suggests that Cu^{II} concentrations of the order of few percent cannot be revealed by XANES. More quantitative conclusions on this fundamental point will be extracted from (i) EXAFS data (*vide infra* section 3.1.2), where it will be shown that both Cu−O distance and Cu coordination number are typical of Cu^+ in zeolites (also here a few percent cannot be detected); (ii) IR results (*vide infra* section 3.2), where the use of appropriate probe molecules will detect the presence of Cu^I species and prove the nearly total absence of Cu^{II} species; (iii) UV−vis spectroscopy (*vide infra* section 3.3), where the absence of absorptions in the region of the d−d transitions will discard the presence of significant amounts of Cu^{II} species; (iv) EPR measurements (*vide infra* section 3.4), where we will definitively estimate to 0.9% of the total copper the amount of Cu^{II} species.

TABLE 1: EXAFS Results for First-Shell Bonding Parameters: *N*, Cu^I Coordination Number; *R*, Cu−O Bond Length; *σ*, Mean-Square Relative Cu−O Displacement, the Corresponding Value for the Cu_2O Model Compound (from Which Phases and Amplitudes Have Been Extracted) Being $\sigma = (6.8 \times 10^{-2}) \pm 10^{-2}$ Å

sample condition	$N \pm 0.3$	R ± 0.02 (Å)	$\sigma \pm 1.010^{-2}$ (Å)
vacuum	2.5	2.00	7.3×10^{-2}
$+N_2$	2.5	2.00	7.3×10^{-2}

The experimental XANES spectrum of Cu-ZSM-5 after N_2 dosage seems to be nearly identical to that measured *in vacuo*; see Figure 2a. This suggests that XAFS is not able to reveal the formation in Cu-ZSM-5 of $Cu^I(N_2)$ adducts at room temperature. This result is also confirmed by the EXAFS analysis, because the first-shell Cu^I environment is not appreciably modified by N_2 dosage (*vide infra* Table 1). As the $Cu^I(N_2)$ adducts formation in Cu^I-zeolites has been, on the contrary, recently observed by IR spectroscopy at room temperature by Kuroda *et al.* on Cu-mordenites (see refs 15 and 57) and by us on Cu-ZSM-5, (see ref 4 and *vide infra* section 3.2.2), we conclude that the weakly bonded $Cu^I(N_2)$ adduct is not stable enough at 300 K under the X-ray beam to be observed by XAFS spectroscopy.

On the contrary, the dosage of CO strongly modifies the Cu^I environment, as clearly documented in Figure 2b, where the pre- and near-edge region spectra after CO dosage at increasing equilibrium pressures on Cu^I-ZSM-5, previously outgassed in vacuum conditions, are reported. The clear stepwise evolution of the XANES spectra as a function of the CO pressure is likely associated with the adsorption process: $Cu^I \xrightarrow{CO} Cu^I(CO) \xrightarrow{CO} Cu^I(CO)_2$ in agreement with the well-known fact that $Cu^I(CO)_n$ ($n = 1, 2$) stable species are formed at *RT* upon CO contact; see refs 17, 21, and 58 and *vide infra* section 3.2.1.

The energy resolution of the monochromator in the adopted experimental conditions being of about 2 eV, no quantitative information from the XANES part of the spectra can be extracted. Despite this limitation, the qualitative information obtained so far is very important because it allows one to conclude that: (i) Cu^I species are predominant and (ii) they add CO ligands with formation of $Cu^I(CO)_n$ ($n = 1, 2$) adducts. These data will be strongly confirmed by other techniques (*vide infra*).

3.1.2 EXAFS Results. Figure 3 reports, in the EXAFS region, the experimental *μx* spectra of the Cu^I-ZSM-5 sample collected

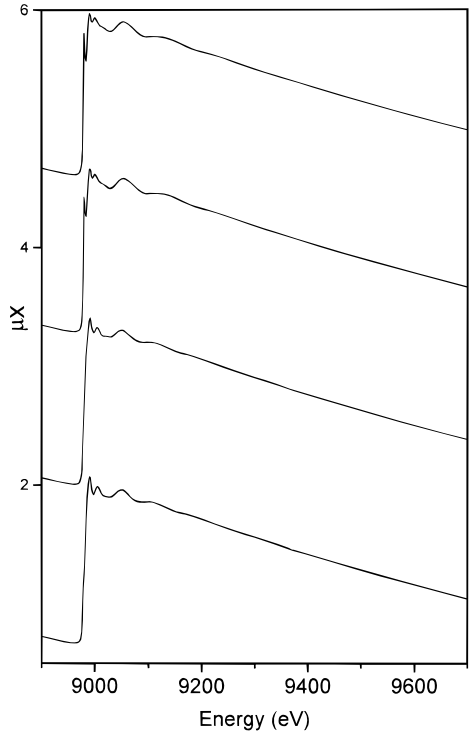

Figure 3. Experimental μx spectra, in the extended region. (from top to bottom) Cu^I-ZSM-5 *in vacuo*; Cu^I-ZSM-5 after interaction with N_2 (equilibrium pressure ≃300 Torr); Cu^I-ZSM-5 after a first dose of CO (equilibrium pressure ≃1 Torr); Cu^I-ZSM-5 after a second dose of CO (equilibrium pressure ≃100 Torr).

in vacuum and after the interaction with different adsorbates. For reasons explained below, in this contribution we only present the EXAFS analysis of the sample in vacuum conditions and in the presence of N_2. Let us notice first that from a simple view of these spectra, the quality of the data is evident, so confirming the homogeneity of the prepared samples as already directly controlled by radiographic methods. This quality becomes even more evident by considering that some glitches, clearly visible on both I_0 and I_1 currents (not shown for brevity) are totally compensated in the computation of $\mu x = \log(I_0/I_1)$. However, the extraction of the corresponding $\chi(k)$ functions has been far from trivial in all cases. In fact, the computed $\chi(k)$ function has been found to be dramatically dependent upon the first point of the interval selected for the interpolation of the atomic absorption; moreover, in all cases we were dealing with an unsubtracted low-frequency component, giving rise upon Fourier transform (FT) calculation to a nonphysical peak at low r values. We have thus decided to operate systematically in the following way: $\chi(k)$ has been computed by simulating the atomic absorption with E^4, E^5, and E^6 polynomial functions and by four cubic splines. For all the four approaches, several different extractions have been systematically computed by changing the first point of the interval used for determining the atomic adsorption. Among all the so-obtained $\chi(k)$ functions, we have immediately discarded all those showing a non-null profile at high k; we are thus normally dealing with about 10 remaining $\chi(k)$ functions (in all cases, vacuum and + N_2, + CO). By carefully superimposing those functions (for each case), we have found that all $\chi(k)$ are totally superimposed in the range 3−13 $Å^{-1}$, while their feature for $k < 3$ $Å^{-1}$ is extraction dependent (for $k > 13$ $Å^{-1}$ the signal is vanishing and we are mainly dealing with noise). The total EXAFS analysis has thus been carried out on four $\chi(k)$ functions arbitrarily chosen among those previously selected (about 10). In all cases $\chi(k)$ has been FT transformed in the extraction independent range 3−13 $Å^{-1}$; all corresponding FT show an unreal peak centered below 1 Å, which is, however, completely separated from the real first-shell peak, so preventing any interference in the back FT between the two signals. For both Cu^I-ZSM-5 in vacuum and in N_2 atmosphere, the results of the EXAFS analysis performed on the four different extractions give rise, within one-third of the reported error bars (*vide infra* Table 1), to equivalent results; for sake of brevity we only report the data obtained from the $\chi(k)$ function extracted using the E^5 polynomial function. Let us remember that the problem of a total removal of low-frequency components is typical of EXAFS spectra generated by atoms having a low backscattering power like oxygen, and it is particularly relevant for the Cu−O system, as can be seen in most FT reported in the quoted references.

Experimental $k\chi(k)$ of the sample in vacuum conditions is shown in Figure 4a. The absence of any beats in the oscillations of the EXAFS function suggests that the main contribution to the overall signal is due only to one coordination shell. In fact, k^3-weighted FT calculated in the range 3−13 $Å^{-1}$ (see Figure 4b) shows only one prominent real peak located at *ca.* 1.6 Å without any correction for the phase shift. No contribution in the typical range of Cu−Cu bond distance was observed. This result clearly confirms the absence of copper clusters in the sample.

The main contribution was then filtered in the range 1.0−2.2 Å and modeled as a Cu−O coordination shell, (using phases and amplitudes extracted from the Cu_2O model compound) resulting in a first coordination shell formed by *ca.* 2.5 oxygen atoms at *ca.* 2.00 Å (*vide infra* section 3.5). When the same contribution is modeled as Cu−Cl, the first coordination shell is given by 1.4 Cl atoms at 2.11 Å. Anyway, after performing an F-test on both fit results (see experimental section), we can discard the second solution with a confidence level higher than 90%. The quality of the fit modeled as the Cu−O coordination shell can be appreciated in parts c and d of Figure 4, where the differences between experimental data and fit is reported in k-space and in r-space (modulus and imaginary parts), respectively. The absence of any relevant amount of Cl in the first shell of copper is definitively demonstrated by the application of the Lee and Beni criterium.[59,60] Taking $\chi_0(k)$ as the extracted $\chi(k)$ (reported in Figure 4a) whose abscissa values have been corrected by considering the energy shift ΔE obtained from the fit reported in Figure 4c,d and taking $\delta(k)$ as the phase extracted from Cu_2O and used in the same fit, we can obtain the phase-corrected radial distribution in the following way (refs 59, 60)

$$D(r) = \int_3^{13} \chi_0(k)\, e^{2ikr}\, e^{i\delta(k)}\, dk \qquad (1)$$

where the integration limits have been given in $Å^{-1}$. The result of this operation is reported in part e of Figure 4, where both the modulus, $|D(r)|$, and the imaginary part, $\mathrm{Im}(D(r))$, of $D(r)$ are reported. From Figure 4e, it is evident that the maximum of $\mathrm{Im}(D(r))$ is coincident with that of $|D(r)|$ (occurring at the correct distance 2.00 Å) and that $\mathrm{Im}(D(r))$ is totally symmetric with respect to the maximum of $|D(r)|$. This can be interpreted only in terms of a first Cu^+ shell composed only by atoms of the same type and located at the same distance. The Lee and Beni criterion[59,60] can be simply explained by remembering that FT is a linear operator and that if two different atoms contribute to the first-shell signal, both real and imaginary parts of the FT of the measured $\chi(k)$ are obtained as a linear combinations of the corresponding functions of the single atoms, but the same does not occur for the modulus, which is given by the square root of the squared sum of real and imaginary parts. If a second atom would be present in the first coordination shell of copper,

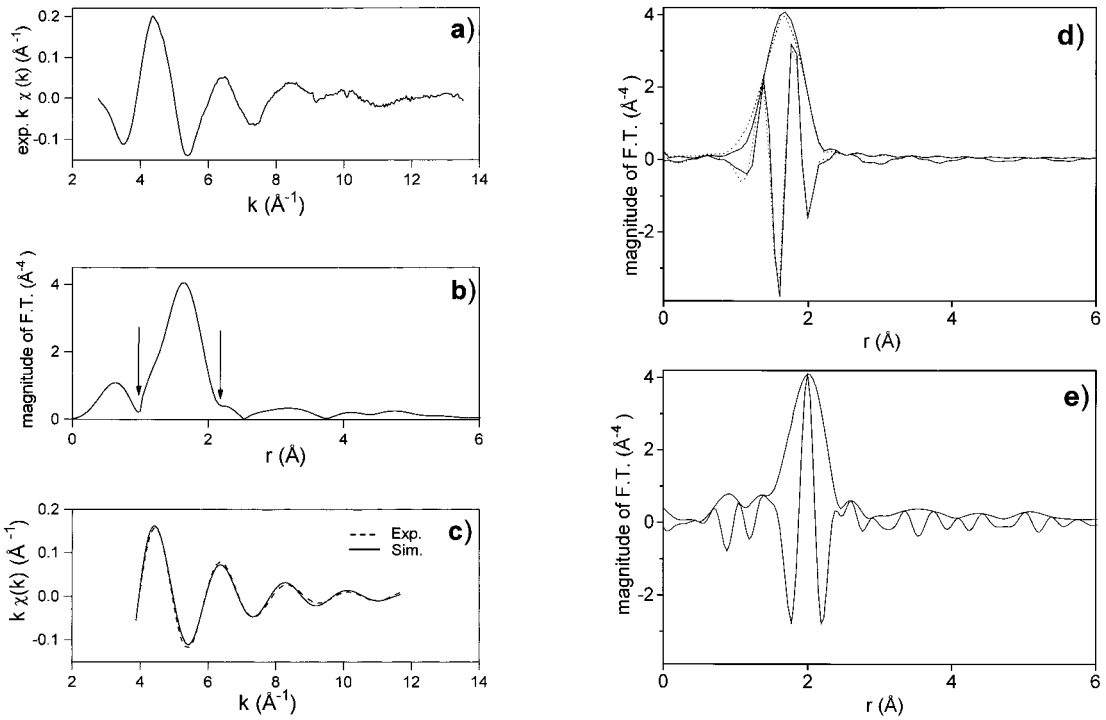

Figure 4. (a) Experimental $k\,\chi(k)$ averaged over the three spectra collected on Cu^I-ZSM-5 in vacuum conditions; (b) k^3-weighted Fourier transform in the range 3−13 Å^{-1} (no phase correction has been adopted; vertical arrows indicate the adopted filtering range; (c) corresponding back-FT of the filtered first-shell data in the 1.0−2.2 Å range (dashed line) and best fits (full line) shell contribution; (d) comparison between experimental (dashed lines) and simulation (full lines) in *r*-space, moduli and imaginary parts of FT; (e) modulus and imaginary part of the phase-corrected k^3-weighted FT in the range 3−13 Å^{-1} following eq 1.

then we should have observed in Figure 4e an asymmetry between Im($D(r)$) and the maximum of $|D(r)|$. In conclusion, from these data the presence of unreacted CuCl is discarded. This result will be supported by both UV−vis DRS and photoluminescence measurements (*vide infra* section 3.3).

In agreement with the EXAFS results obtained by Liu and Robota,[38] and those obtained by us in previous investigations[4,20,21] using other techniques, the resulting Cu−O coordination number is, within error, consistent with the presence of 2,3-coordinated Cu^I ions in the zeolite cages (*vide infra* section 3.5). Both coordination number and Cu-O distance reported in Table 1 are in agreement with the data reported in literature concerning the Cu^I ions present in zeolites (see ref 15, sample activated at 873 K), while all Cu^{II} species are usually characterized by a higher coordination number (typically ≃4) and by a lower Cu−O bond length (typically ≃1.95 Å).[15,18,19,46] Only Yamashita *et al.*,[41] report a higher Cu−O bond length in Cu^{II}-ZSM-5 (2.00 Å) than in Cu^I-ZSM-5 (1.94 Å); however, error bars have not been reported in that work.

The EXAFS analysis of the Cu^I-ZSM-5 after N_2 dosage yields, within the experimental errors, the same results obtained by the sample measured *in vacuo*; see Table 1.

The interaction of CO with Cu^I sites in Cu^I-ZSM-5 is described in Figure 5. Part a shows the $k\chi(k)$ functions of the Cu^I-ZSM-5 in vacuum and under a CO equilibrium pressure of 1 Torr. The strong deformations induced on the $k\chi(k)$ function by the CO dosage are evident, both on the signal amplitude and on the period of the EXAFS oscillations: this undoubtedly proves that EXAFS is able to detect the formation of $Cu^I(CO)_n$ adducts in Cu^I-zeolites at room temperature. FT transforms of the $\chi(k)$ functions in the range 3−13 Å^{-1} are reported in part b. The radial distributions show now the evident contribution of two shells. The first peak contains the contributions due to both framework oxygen and C atom(s) of CO, while the second is due to the oxygen(s) contribution of CO group(s). The FT, performed without any phase corrections, shows the two peaks

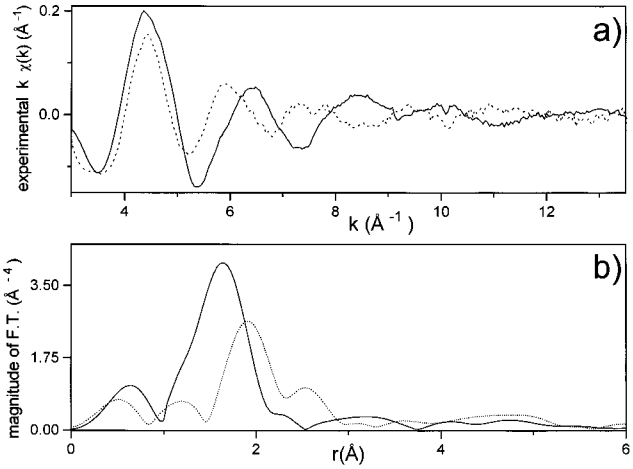

Figure 5. Effect of CO dosage, equilibrium pressure ≃1 Torr (dotted line curves), on the virgin sample (full line curves): (a) on the $k\,\chi(k)$ functions; (b) on the corresponding k^3-weighted FT in the range 3−13 Å^{-1} (no phase correction has been adopted). Interaction with CO strongly modifies the environment of Cu^I cations, as documented by variation of both intensity and period of the $\chi(k)$ oscillations and by the great modifications observed in the corresponding FT. Note, however, that the decrease of intensity and the displacement to higher *r* of the first-shell peak are probably due to an interference effect between the Cu−O and Cu−C signals, whose corresponding Δr is probably too small (≃0.1−0.2 Å) to be resolved with the adopted Δk interval.

at ≃1.9 and 2.5 Å, respectively. The overlap between first and second shell contributions prevents the possibility of performing a separate analysis. These data cannot be analyzed by using the single-scattering approximation utilized to extract the data concerning the sample in vacuum and reported in Table 1. In fact, both theoretical contribution[61] and several IR experiments performed on CO adsorbed on monovalent cations in zeolites[62−64] strongly suggests that carbon monoxide predominantly forms, under the adopted conditions, linear adducts (through the carbon

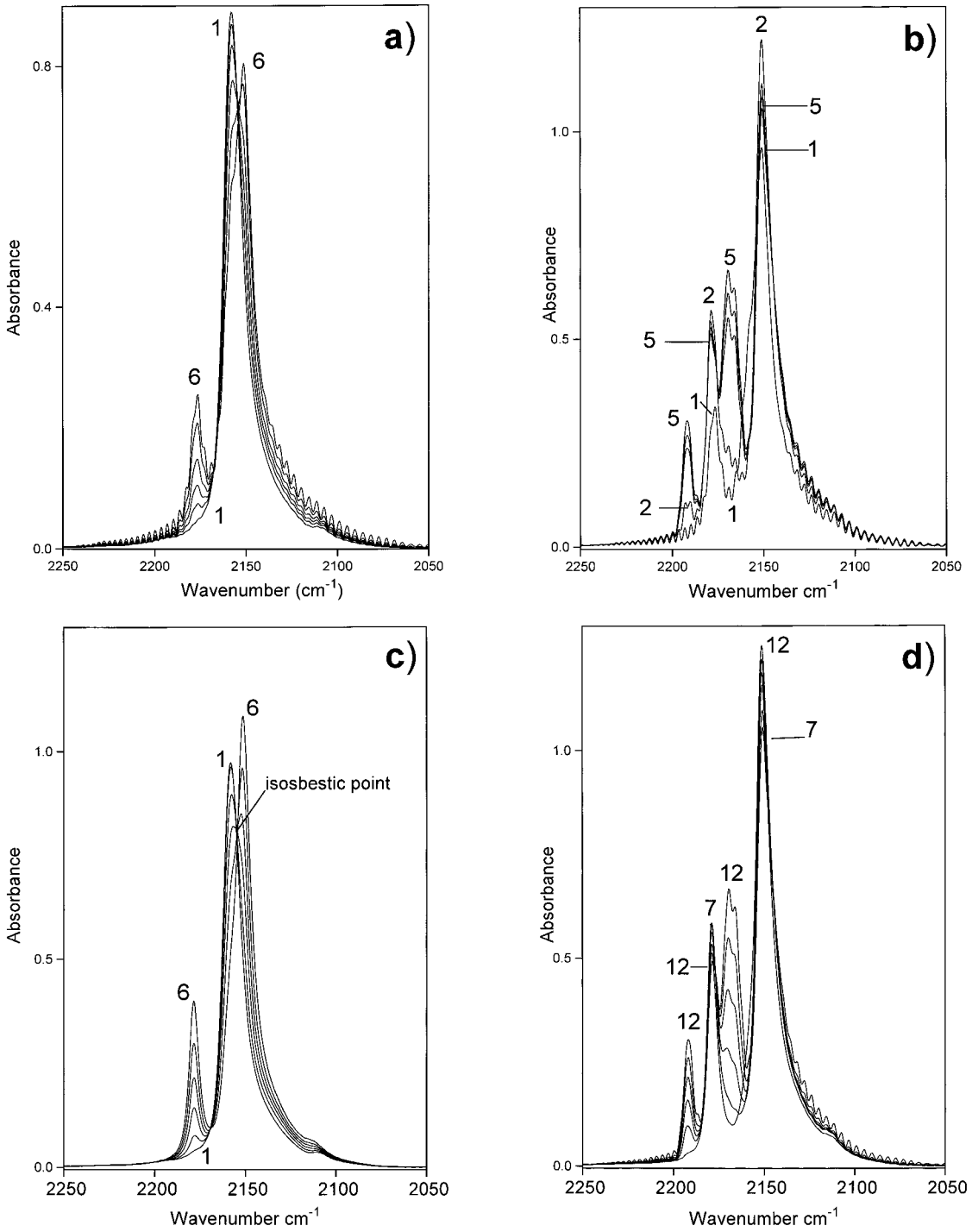

Figure 6. IR spectra of CO interacting with Cu^I sites. (a) Spectra collected at 300 K at equilibrium pressures ranging from ≃0.1 (spectrum 1) to 10 Torr (spectrum 6); (b) spectra collected at constant pressures (≃10 Torr) and decreasing temperatures from 300 (spectrum 1) to ≃110−120 K (spectrum 5); (c, d) spectra collected at ≃110−120 K at equilibrium pressures ranging from ≃0.1 (spectrum 1) to 10 Torr (spectrum 12).

atom) with monovalent centers ($X^+\cdots C-O$). In this linear geometry the effects due to multiple scattering[65,66] are enhanced by focusing effect of the central intervening atom.[67] The analysis of these data in the framework of the multiple-scattering theory[70−72] is in progress and will be reported in a subsequent contribution.[73]

3.2 IR Results. IR spectroscopy is widely applied to investigate the adsorption of small probe molecules into zeolites cavities or channels with the aim of characterizing the cationic sites structure.[4,15,20,21,40,43,62,63,74−87] Here we discuss the interaction of CO, N_2, and NO with Cu cations in ZSM-5.

3.2.1 Vibrational Spectra of $Cu^+\cdots(CO)_n$ ($n = 1, 2, 3$). The IR spectra of CO adsorbed on Cu^I-ZSM-5 are shown in Figure 6 parts a−d. At 300 K and at lowest CO coverage (see curve 1 in part a of Figure 6), the typical band at 2157 cm^{-1} due to the $Cu^I(CO)$ complex is observed.[17,21,58] By increasing the CO pressure the 2157 cm^{-1} band is progressively eroded, while two strong and distinct bands at 2178 and 2151 cm^{-1} grow in a proportional way. We assign the 2178 and 2151 cm^{-1} bands to the symmetric and asymmetric stretching modes of the $Cu^I(CO)_2$ complex, respectively.[21] The evolution of these bands upon increasing the CO pressure indicates that the transformation of $Cu^I(CO)$ into $Cu^I(CO)_2$ species is progressively taking place and becomes nearly complete at $P = 10$ Torr (only a weak residue of the original 2157 cm^{-1} band is remaining). The total consumption can be achieved at *RT* only with higher equilibrium

SCHEME 1

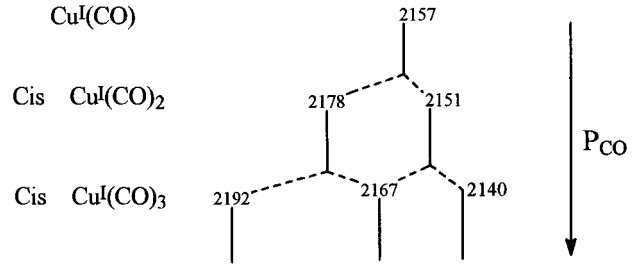

pressures (spectra not reported for clarity). This phenomenon has also been evidenced, although only in a qualitative way, in the XANES and EXAFS spectra (*vide supra* Figures 2b and 5).

It is interesting to note that while the $Cu^I(CO)_2$ complexes, responsible for the 2178 and at 2151 cm^{-1} bands, are completely destroyed by outgassing the sample at *RT*,[21] the monocarbonylic band at 2157 cm^{-1} shows an irreversible character at 300 K. The stability of the $Cu^I(CO)$ bond at *RT* has also been confirmed by the XANES technique (*vide supra* Figure 2b). This fact, together with the corresponding hypsochromic shift ($\Delta\tilde{\nu} = +14$ cm^{-1} with respect to the 2143 cm^{-1} frequency of the CO molecule in the gas phase[88]), evidences an important σ-dative contribution in the Cu^+-CO bond.[21] By studying photoemission and thermal desorption spectroscopy of CO adsorption on a Cu_2 O(100) single crystal, Cox and Schulz[89] pointed out the importance of the σ-donation in the Cu^+-CO. However, in a recent review,[90] Salomon *et al.* showed that beside the important role played by σ-donation there is also experimental evidence of π-back-donation; the same conclusion has also been reached in the very recent theoretical contribution of García *et al.*[91]

The capacity of Cu^I to coordinate ligands to complete its coordination sphere is not exhausted with the formation of $Cu^I(CO)_2$ species. This fact is clearly visible in Figure 6b, where we have initially dosed 10 Torr of CO at *RT* and then gradually lowered the temperature up to ≃110−120 K at constant CO pressure. During the temperature decrease, the formation of $Cu^I(CO)_3$ complexes by addition of CO to the pre-existing $Cu^I(CO)_2$ dicarbonyls is evident, from the new bands at 2192 and 2167 cm^{-1} and the parallel decrease of the 2178 cm^{-1} dicarbonyls component. The 2167 cm^{-1} band appears to consist of a doublet; this means that we are, most probably, dealing with two families of very similar tricarbonyl species formed on slightly different Cu^I sites. The tricarbonyl structure is not only associated with the 2192−2167 cm^{-1} pair but also with a shoulder at ≃2140 cm^{-1} (strongly overlapped to the $\tilde{\nu}_{asym}$ mode of the $Cu^I(CO)_2$ complex at 2151 cm^{-1}. The same phenomenon is even better illustrated in Figure 6c,d, where the adsorption of CO at constant temperature (≃110−120 K) is studied as a function of the CO equilibrium pressure. A schematic representation of the vibrational modes of the Cu^I (CO), $Cu^I(CO)_2$, and $Cu^I(CO)_3$ adducts in Cu^I-ZSM-5 formed upon stepwise addition of CO to Cu^I is given in Scheme 1.

The overlap of one of the dicarbonyl modes, $\tilde{\nu}_{asym}$(CO) at 2151 cm^{-1}, with the lowest frequency mode of Cu^I $(CO)_3$, ≃ 2140 cm^{-1}, explains why the absorption in the 2130−2165 cm^{-1} range does not undergo to the same decrease as that observed for the $\tilde{\nu}_{asym}$(CO) at 2178 cm^{-1} band of the dicarbonyl modes during the $Cu^I(CO)_2 \xrightarrow{CO} Cu^I(CO)_3$ step. The fact that the $Cu^I(CO)_3$ complex is associated with three different C−O stretching frequencies implies that the three CO molecules are not equivalent (otherwise only two bands should be expected). This means that the symmetry of the $Cu^I(CO)_3$ complex is less than C_{3v}. The ability of Cu^I to give $Cu^I(CO)$, $Cu^I(CO)_2$, and $Cu^I(CO)_3$ complexes, characterized by C−O stretching frequencies in the 2200−2150 cm^{-1} region, has been very recently reported in ref 92. In homogeneous conditions the symmetry of $Cu^I(CO)_2$ and $Cu^I(CO)_3$ species is $D_{\infty h}$ and D_{3h}, respectively.[92] In the zeolite, the linear and the planar configurations are not possible because of the steric hindrance of the wall channels, and lower symmetries are adopted.

It must be noticed that the ability of Cu^I cations to increase their coordination sphere through coordination of up to two or three ligands is in full agreement with the low coordination number (and the high coordinative unsaturation) of Cu^I ions as obtained by EXAFS analysis (*vide supra* Table 1).

A further important observation must be made: while both at *RT* and at ≃110−120 K the $Cu^I(CO) \xrightarrow{CO} Cu^I(CO)_2$ transformation is total, the same does not occur at ≃110−120 K for the $Cu^I(CO)_2 \xrightarrow{CO} Cu^I(CO)_3$ transformation. In fact, the 2178 and at 2151 cm^{-1} bands are not completely eroded upon increasing the CO equilibrium pressure. This fact cannot be ascribed to an insufficient amount of dosed molecules, because an increase of the equilibrium pressure, at the investigated temperature (≃110−120 K), does not appreciably modify the situation. By systematically performing a band deconvolution on the whole set of spectra reported in Figure 6c,d, we were able to follow the evolution of the integrated intensity of the band(s) of the $Cu^I(CO)$, $Cu^I(CO)_2$ and $Cu^I(CO)_3$ complexes as a function of the CO equilibrium pressure. Deconvolutions have been performed with a home-developed software (ASYMGRAD) already described elsewhere,[93,94] which uses the minimization capabilities of MINUIT.[34] The ratio between the maximum value reached by the integrated intensity of the bands attributed to the $Cu^I(CO)_2$ complex and the value reached in the spectrum collected at the highest CO pressure is about 2. From these data, it is evident that at ≃110−120 K the decrease of the integrated intensity of the 2178−2151 cm^{-1} pairs is only about 50%, so suggesting that we are probably dealing with two different families of Cu^I sites differing in the fact that only one is able to coordinate, at ≃110−120 K, three CO molecules. If this interpretation holds, we have two nearly equipopulated families of Cu^I sites characterized by two different coordinative unsaturations (see Note Added in Proof). We will hereafter label the less unsaturated family of sites (able to coordinate at ≃110−120 K up to two CO molecules) as site **I** and the more unsaturated family of sites (able to coordinate at ≃110−120 K up to three CO molecules) as site **II**. We shall see in the following that this conclusion will be strongly supported by photoluminescence measurements and computer graphics simulations (*vide infra* sections 3.3 and 3.5, respectively). At this point, it is evident that the coordination number of Cu^I cations obtained by EXAFS analysis ($N = 2.5 \pm 0.3$) is the result of two signals generated by Cu^I cations in sites **I** and **II** having a higher and a lower *N* value, respectively.

3.2.2 Vibrational Spectra of $Cu^+(N_2)_n$ ($n = 1$). Cu^I-exchanged zeolites represent a rare example of a system capable of adsorbing N_2 at *RT* with formation of $Cu^I(N_2)$ stable complexes (see refs 15 and 57 for Cu-mordenites and ref 4 for Cu-ZSM-5). The IR spectra of N_2 adsorbed on Cu^I cations of the zeolite are reported in Figure 7 (at 300 K in part a and at ≃110−120 K in part b). The sharp and well-defined band at 2295 cm^{-1} ($\Delta\tilde{\nu}_{1/2} = 9.0-5.5$ cm^{-1}) is the $\tilde{\nu}_{NN}$ of the $Cu^I(N_2)$ complex. This frequency is similar to that found by Kuroda *et*

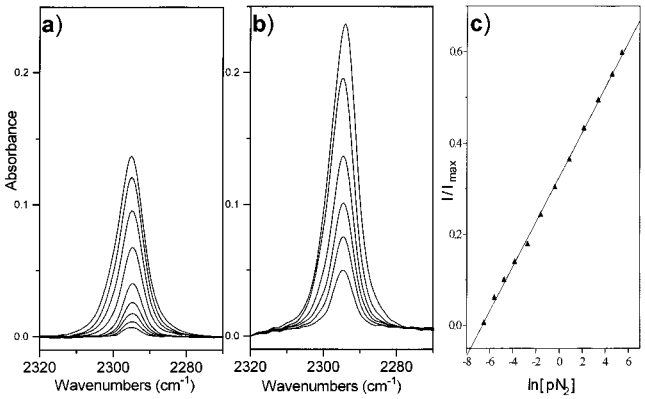

Figure 7. IR spectra of N_2 adsorbed on Cu^I-ZSM-5. (a) spectra taken at 300 K and corresponding to equilibrium pressures ranging from $\simeq 10^{-3}$ to 175 Torr; (b) spectra collected at $\simeq$110−120 K (equilibrium pressures $\simeq 2.0 \times 10^{-3}$ to 175 Torr); (c) Temkin plot of the 300 K optical isotherm corresponding to the spectra reported in part a: integrated intensity of the N−N stretching band of the $Cu^I(N_2)$ adduct normalized to the intensity of the same band at 175 Torr (I/I_{max}) *vs* logarithm of N_2 equilibrium pressure.

SCHEME 2

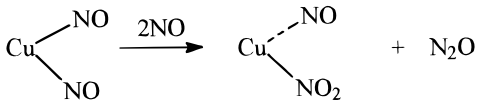

al. on Cu-mordenite[15,57] (2299 cm^{-1}). The dependence of the $\Delta\tilde{\nu}_{1/2}$ values of the 2295 cm^{-1} $Cu^+(N_2)$ band as a function of the N_2 coverage (θ), see Figure 7, shows values ranging from 9.0 cm^{-1} ($\theta \simeq 1$) to 5.5 cm^{-1} ($\theta \simeq 0$). While these $\Delta\tilde{\nu}_{1/2}$ values are quite small compared with those usually observed for surface species on heterogeneous systems, they are definitely larger than 1.5−2.0 cm^{-1} (the $\Delta\tilde{\nu}_{1/2}$ values observed for dinitrogen−transition-metal adducts in low-temperature matrices[95]). This behavior can only be explained by assuming the presence of slightly different copper sites (*vide infra* section 3.5). This hypothesis is fully compatible with the Temkin plot reported in Figure 7c (normalized integrated intensity of the dinitrogen stretching band of the $Cu^+\cdots N{-}N$ adducts at *RT vs* the logarithm of the corresponding N_2 equilibrium pressure), which can be satisfactory fitted using one line only as expected for an adsorption process concerning energetically nonequivalent sites.[96] From the above experiment, it emerges that we cannot separate the spectroscopies of N_2 adsorbed on sites **I** and **II**; however, it is quite conceivable that the species stable at *RT* are preferentially formed on sites **II**, due to its higher polarizing power.

As a final remark on the IR spectra of CO and N_2 adsorbed on Cu^I-ZSM-5, we underline that both probe molecules have not detected the presence of extralattice Al^{3+} species. In fact, the bands at $\simeq$2220 cm^{-1} and at $\simeq$2350 cm^{-1}, typical of $Al^{3+}\cdots$-CO[62,63,97] and of $Al^{3+}\cdots N_2$[98] adducts, respectively, have not been observed. These data are in agreement with the IR spectra of the zeolite in the OH stretching region reported in Figure 1, where no $\tilde{\nu}$(OH) band associated with extralattice Al^{3+} species was observed. This is a further proof of the high structural quality of the investigated sample.

3.2.3 Vibrational Spectra of $Cu^+(NO)_n$ ($n = 1, 2$). The study of the basic coordination chemistry of the Cu^I sites (**I** and **II**) toward NO is complicated by the decomposition reaction which is already taking place at *RT* with initial formation of N_2O and Cu^{II} $(NO)(NO_2)$ species following the path represented in Scheme 2 (see the work of Spoto *et al.*[21] and related discussion). For this reason the dosages of NO on Cu^I-ZSM-5 have been made following a procedure different from that experimented for CO. In order to suppress as much as possible the decomposition reaction, the NO was dosed on a sample formally at 77 K (actually at $\simeq$110−120 K) in the 7×10^{-2}−7×10^{-1} Torr pressure interval (Figure 8). The band at 1812 cm^{-1}, due to the $Cu^I(NO)$ mononitrosylic complex,[2,11,20,21,81,82] is predominant at low NO dosages, while the symmetric stretching (1827 cm^{-1}) and asymmetric stretching (1734 cm^{-1}) of the $Cu^I(NO)_2$ dinitrosylic species[2,11,20,21,81,82] take over with increasing NO coverage at the expense of the previous band. The half-widths of the symmetric and asymmetric stretching of the $Cu^I(NO)_2$ adduct ($\Delta\tilde{\nu}_{1/2}$ 10 and 17 cm^{-1}, respectively) is well comparable with that observed in nitrosylic complexes of known stoichiometry in solution.[99] No evidence of formation of $Cu^I(NO)_3$ complexes is present in the spectra reported in Figure 8. This is not surprising because, even if CO and NO molecules have nearly the same dimensions, in the $Cu^+\cdots(CO)_n$ interaction each probe molecule shares two electrons (giving rise to a total number of six shared electrons for $n = 3$), while in the $Cu^+\cdots(NO)_n$ interaction each probe molecule shares three electrons (resulting in the same total number of shared electrons for $n = 2$). This simple consideration qualitatively explains why sites **II** have no tendency to adsorb a third NO molecule even if there are no steric constraints. This in turn means that the NO probe is not able to distinguish between copper sites **I** and **II** as was the case for carbon monoxide.

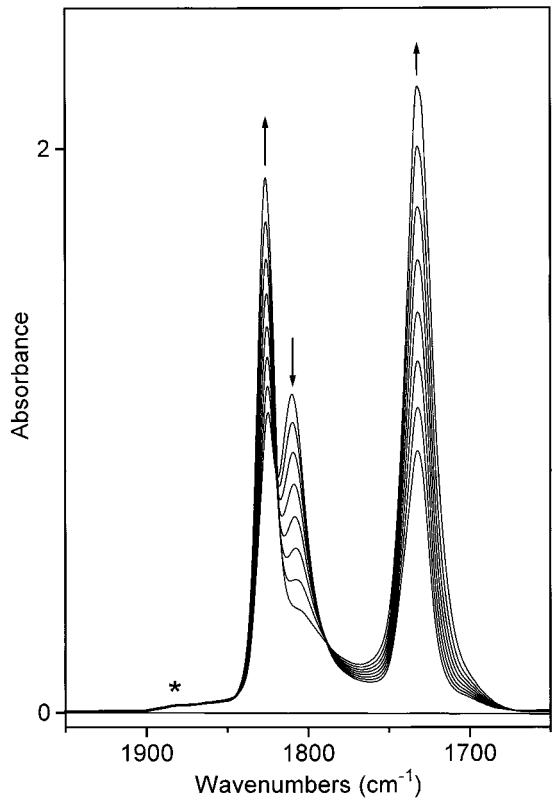

Figure 8. IR spectra of increasing doses of NO dosed on Cu^I-ZSM-5 at $\simeq$110−120 K (equilibrium pressures ranging from $\simeq 7 \times 10^{-2}$ to 7×10^{-1} Torr). The arrows indicate the progressive evolution from mono- into dinitrosil species upon increasing NO coverage also evidenced by the two isosbestic points at 1820 and 1790 cm^{-1}. The * indicates the weak absorption in the 1915−1890 cm^{-1} range due to NO molecules adsorbed on Cu^{II} cations; the line indicates the background before NO dosage.

NO adsorbed on Cu^{II} species in zeolites would give rise to absorption in the 1915−1880 cm^{-1} interval (see refs 11, 21, and 81 and *vide infra*): consequently, this band being nearly totally absent in the spectrum reported in Figure 8, it can be concluded that IR of adsorbed NO on the virgin sample

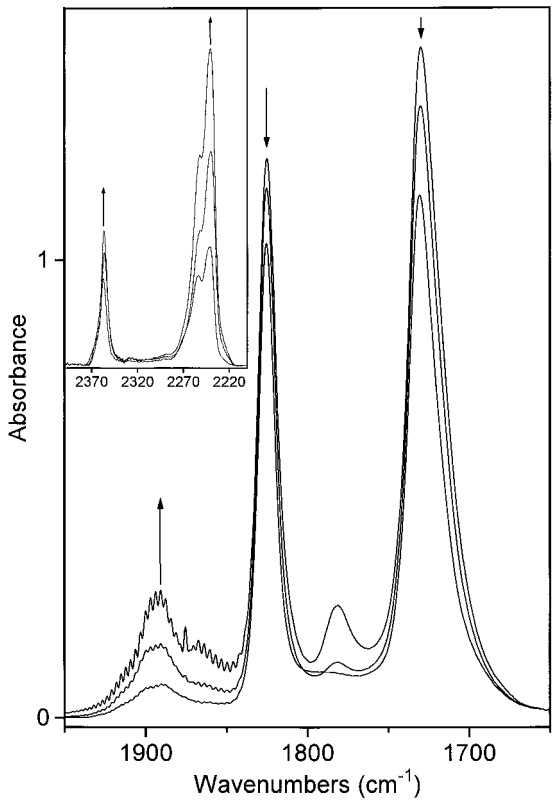

Figure 9. Spectra of NO adsorbed on Cu^{I}-ZSM-5 at ≃110−120 K in the 1−8 Torr pressure interval. The arrows indicate the progressive decrement of $Cu^{I}(NO)_2$ in favor of $Cu^{II}(NO)$ species and the correlated formations of weakly bonded N_2O and $Cu^{II}(N_2)$ adducts (see inset).

givesfurther proof of the nearly total absence of Cu^{II} species in samples prepared following our procedure. Only a very weak absorption, having an integrated intensity representing less than 1% of the total area, is observed around 1890 cm^{-1} (in particular, $I_{1890}/I_{1827} = 1.9\%$ and $I_{1890}/I_{1734} = 0.9\%$).[100]

This conclusion has only a qualitative character, since we do not know the extinction coefficient of the $\tilde{\nu}_{NO}$ in $Cu^{II}(NO)$ complexes (which could be much lower than that of Cu^{I} (NO) and Cu^{I} $(NO)_2$ complexes). In order to give a more quantitative estimation of the relative amount of Cu^{II} and Cu^{I} present in our virgin samples, we have designed an experiment where Cu^{II} was formed *in situ* from the pre-existing Cu^{I} by action of NO during the decomposition reaction. The experiment has been carried out in three subsequent steps (indicated in the following as step a, b, and c).

Step a: Increasing doses of NO have been dosed onto the virgin zeolite at ≃110−120 K up to a final NO pressure of about 8 Torr; the corresponding sequence of spectra (see Figure 9) are characterized by the presence of $Cu^{I}(NO)_2$ dinitrosyl (bands at 1827−1734 cm^{-1} already illustrated in Figure 8), by a pairs of bands at 1866 and 1782 cm^{-1} (due to $(NO)_2$ dimers[101] physisorbed on the zeolite channels, not observed in the spectra of Figure 8 due to the considerably lower NO pressure) and by a not negligible absorption at 1915−1880 cm^{-1} due to incipient formation of Cu^{II} $(NO)(NO_2^-)$ generated upon decomposition of $Cu^{I}(NO)_2$ as reported in refs 11, 21, and 81 and demonstrated by the presence of weakly bonded N_2O, as revealed by the presence of an intense peak at 2270−2220 cm^{-1} (see inset of Figure 9). Meanwhile no evidence of $Cu^{I}(N_2O)$ is obtained, due to the lack of absorption at 2293 cm^{-1}.[102] In the same inset, a composite absorption at 2370−2345 cm^{-1} is also evident; we attribute the latter band to N_2 molecules adsorbed on Cu^{II} sites as demonstrated by a parallel experiment of N_2 dosage on Cu^{II}-ZSM-5 (not shown for brevity). As the 2370−2345 cm^{-1} band is complex, a contribution of NO^+ species cannot be excluded.[103] These species could be formed in a less important side process through disproportionation of liquid-like NO into $NO^+ + (N_2O_2)^-$ or into $NO^+ + N_2O + NO_2^-$ ionic species.[104] The absence of the band at 2295 cm^{-1}, previously assigned to $Cu^{I}(N_2)$ adducts (*vide supra* section 3.2.2 and see ref 4), rules out dinitrogen molecules adsorbed on Cu^{I} sites. The formation of N_2 indicates that the NO decomposition into N_2 and O_2 is already initiating following the plausible scheme (Scheme 3) already hypothesized by Spoto *et al.* in ref 21. The N_2 formed *in situ* is initially bonded to the copper(II) center and is then displaced by NO. The concentration of $Cu^{II}(N_2)$ adducts is remarkable only at $T < 373$ K; on the contrary, at temperatures near *RT* the intensity of the $\tilde{\nu}(N_2)$ mode is negligible. The mechanism reported in Scheme 3 is not the only one which can be hypothesized, see, *e.g.*, that proposed by Aylor *et al.*,[77] which however represents a variant of that previously reported by Spoto *et al.*,[21] the first five steps proposed in ref 77 being the same as those reported in ref 21 (steps I−IV). The important point observed here is, however, that during the reaction a transient N_2 species is formed in which N_2 is bonded to Cu^{II} centers and that we have no evidence of $Cu^{I}(N_2)$ complexes, due to the lack of the band at 2295 cm^{-1}.

SCHEME 3

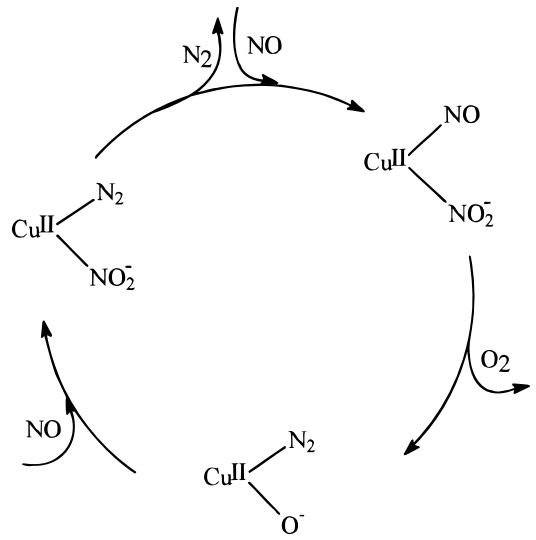

Step b: The sample is now allowed to gradually warm up to 300 K in order to favor the decomposition of NO and the formation of $Cu^{2+}(NO)$ species, to the detriment of the pre-existing $Cu^{+}(NO)_2$ complexes (Figure 10). An intense band attributed to $Cu^{2+}(NO)$ is indeed clearly growing, while the bands due to both $Cu^{I}(NO)$ and $Cu^{I}(NO)_2$ species are decreasing, this proves that the oxidation process of copper sites is proceeding. The thermal dissociation of $(NO)_2$ dimers as a function of the temperature increase is also demonstrated by the total erosion of the 1866−1782 cm^{-1} bands. The evolution of the physically adsorbed N_2O species and of the $Cu^{+}(N_2)$ adducts is reported in the inset of Figure 10 up to the eighth spectrum (at higher temperatures the intensities of the bands decrease due to the thermal instability of the corresponding species).

Step c: The sample is cooled down again at the temperature of step **a** (≃110−120 K), so restoring the temperature and the pressure conditions of the last spectrum of step a (see Figure 9). Comparison of the two spectra is reported in Figure 11a. For all spectra, the ratio between the asymmetric and the symmetric stretching modes of the $Cu^{I}(NO)_2$ adduct was found

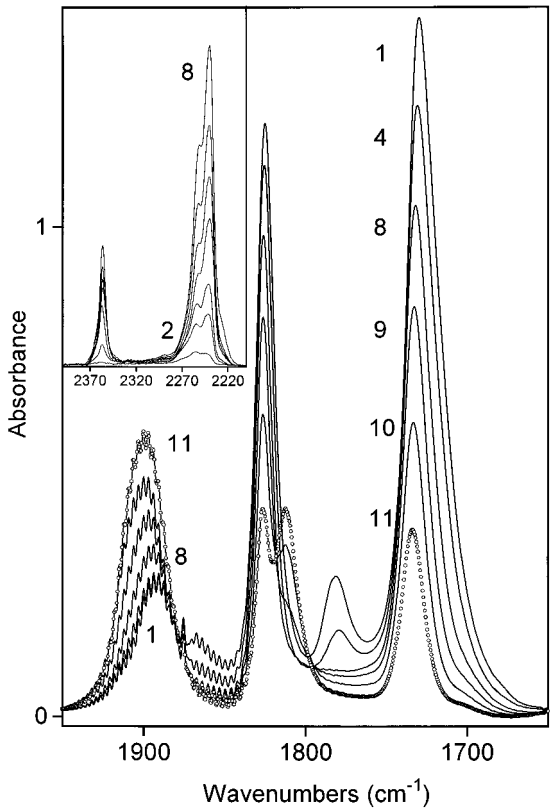

Figure 10. Evolution of the IR spectrum of adsorbed NO at constant pressure (8 Torr) as a function of the temperature, from ≃110−120 K (spectrum 1) up to 300 K (spectrum 11). The inset show the evolution of weakly bonded N_2O species and of $Cu^{II}(N_2)$ adducts.

to be

$$\frac{\epsilon_{Cu^{I}(NO)_2asym}}{\epsilon_{Cu^{I}(NO)_2sym}} = \frac{I_{1734}}{I_{1827}} = 2.2 \qquad (2)$$

By comparing the decrement of the $Cu^{I}(NO)_2$ bands ($-\Delta I_{1827}$ and $-\Delta I_{1734}$) with the increment of the Cu^{II} (NO) band (ΔI_{1890}) we are able to estimate the ratio between the extinction coefficients of the two adducts

$$\frac{\epsilon_{Cu^{I}(NO)_2asym}}{\epsilon_{Cu^{II}(NO)}} = -\frac{\Delta I_{1734}}{\Delta I_{1890}} = 1.1 \qquad (3)$$

and

$$\frac{\epsilon_{Cu^{I}(NO)_2sym}}{\epsilon_{Cu^{II}(NO)}} = -\frac{\Delta I_{1827}}{\Delta I_{1980}} = 0.5 \qquad (4)$$

The quantitative estimates of the values of ΔI have been obtained by performing the band fitting on the spectra shown in Figure 11a using ASYMGRAD.[93,94] In order to perform a correct evaluation, the fit has been performed in the range 1950−1650 cm^{-1} (thus also on the bands at 1866 and 1782 cm^{-1} of the dimeric $(NO)_2$ species). All bands have been simulated using full Lorentzians functions. The quality of the fits is visible in parts b and c of Figure 11 and is quantitatively supported by the fact that in both cases the ratio between the $(NO)_2$ bands intensity is $\Delta I_{1782}/\Delta I_{1866} = 4$, in full agreement with the recent data reported by Kometer *et al.*[101] in $(NO)_2$ isolated in Ne matrix ($\Delta I_{1779}/\Delta I_{1865} = 4.6 \pm 0.5$). From the datum reported in eqs 3 and 4, it is inferred that the original very weak peak observed in the 1915−1880 cm^{-1} region of Figure 8 is due to NO molecules adsorbed on Cu^{II} cations which correspond to less than 1% Cu^{II} of the total copper sites. From the data reported in Figure 11b,c, we can also conclude that about 28% of the Cu^{I} sites have been oxidized in the experiment described here.

3.3 UV−Vis Spectroscopy. UV−vis spectroscopy has been used to investigate the oxidation and the coordinative state of the copper species and to add further information on the Cu^{II}/Cu^{I} ratio. The possible residual presence of unreacted CuCl molecules or $(CuCl)_n$ microaggregates will also be debated.

The UV−vis−near-IR diffuse reflectance spectrum of Cu^{I}-ZSM-5 collected in vacuum conditions is not reported due to its misleading nature. In fact, due to the luminescence activity of isolated and coordinatively unsaturated Cu^{+} ions upon irradiation with ultraviolet light (*vide infra*), the reflectance instrument, in which the detector is located after the sample, is collecting not only the light scattered by the sample but also the Cu^{+} luminescence emission. As a result, the UV−vis spectrum of Cu-ZSM-5 in vacuum is strongly distorted by the presence of excess reflectance signals at wavenumbers corresponding to the photoluminescence excitation peaks of Cu^{+} (*vide infra* and see ref 21).

This problem can be partially overcome by introducing H_2O or NH_3 molecules in the zeolite, because they quench the Cu^{+} luminescence emission through the complexation of the exposed and easily accessible Cu^{+} ions. This procedure leads to the spectra A and B reported in Figure 12 (in presence of H_2O and NH_3, respectively) characterized by strong absorption bands in the 50000−42000 cm^{-1} (200−240 nm) range, *i.e.* the same interval where charge transfer absorptions are reported to occur in homogeneous conditions for $Cu^{+}(H_2O)_2$ and $Cu(NH_3)_2^{+}$.[21,105] In the inset of Figure 12, an exploded view of the 20000−8000 cm^{-1} (500−1250 nm) range of Cu^{I}-ZSM-5 in presence of NH_3 is reported. In the same inset two spectra collected under the same NH_3 equilibrium pressure of Cu^{II}-ZSM-5, obtained from the same H-ZSM-5 sample after aqueous exchange with $Cu(NO_3)_2$ (spectrum C), and of Cu−Y, where copper metal clusters have been formed into the supercages by reduction of a Cu^{I}−Y sample in CO atmosphere at high temperature[106,107] (spectrum D), are reported for sake of comparison. It is immediately evident that: (i) the presence of Cu^{2+} ions can be safely ruled out because of the absence of bands in the 20000−10000 cm^{-1} (500−1000 nm) range (d−d transitions of Cu^{II} complexes[21,108,109]); (ii) the lack of unreacted $(CuCl)_n$ clusters is demonstrated by the absence of the absorption edge at about 26000 cm^{-1} (385 nm);[21] (iii) finally the presence of possible reduced species (Cu^0) can also be excluded due to the absence of the absorption edge at about 17000 cm^{-1} (590 nm) typical of copper metal clusters.[21,107,110] Due to the low extinction coefficients of d−d bands in Cu^{II} complexes, the sensitivity of the UV−vis spectroscopy in the detection of Cu^{II} is not very high. This is not true for the edge absorptions; hence the presence of Cu^0 and $(CuCl)_n$ can be excluded, in total agreement with the EXAFS results.

Due to its high sensitivity to the Cu^{+} environment, luminescence spectroscopy has also been widely employed in the characterization of Cu^{+} ions in zeolites.[15,41,83,110−115] Figure 13 reports both emission and excitation photoluminescence spectra of Cu^{I}-ZSM-5 collected at *RT* in vacuum conditions. Spectra in the 45 000−25 000 cm^{-1} (222−400 nm) range represent excitation scans performed with the emission monochromator at 20 408 cm^{-1} (490 nm) and at 18 692 cm^{-1} (535 nm). Spectra in the 25 000−12 500 cm^{-1} (400−800 nm) range represent emission scans performed with the excitation monochromator at 39 063 cm^{-1} (256 nm) and at 33 333 cm^{-1} (300 nm). Emission spectra collected at different emission wave-

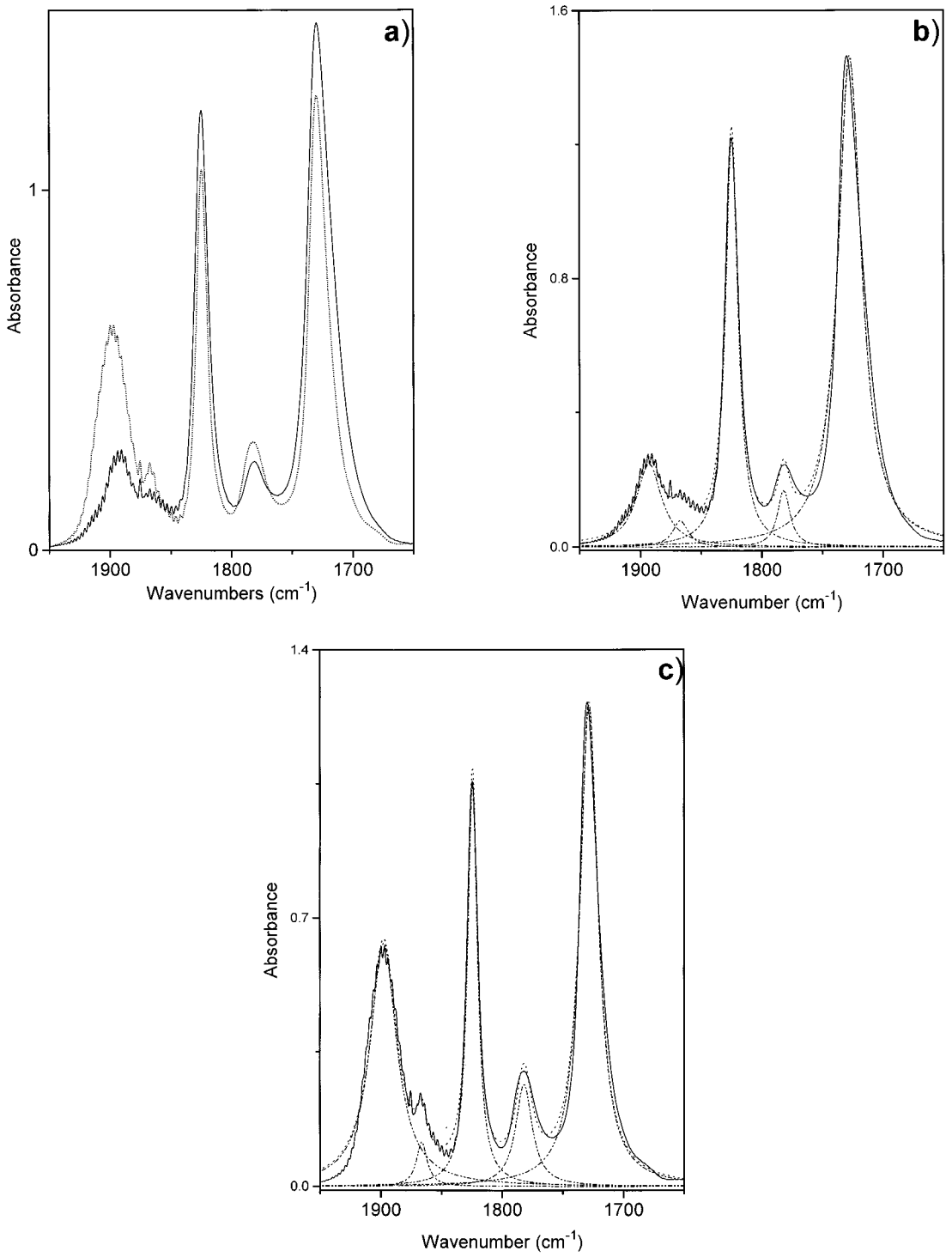

Figure 11. (a) Comparison of the spectrum obtained by cooling down again to ≃110−120 K the sample characterized by spectrum 11 of Figure 10 (dotted line) and the last spectrum of Figure 9 (full line). (b, c) deconvolution of the two spectra reported in part a: experimental spectra (full line), simulated spectra (dotted lines), and resolved Lorentzian components (dot-dashed lines).

numbers clearly show the presence of two predominant peaks at 20 400 cm^{-1} (490 nm) and at 18 700 cm^{-1} (535 nm) respectively; the same holds for excitation scans, which exhibit two evident peaks at 39 063 cm^{-1} (256 nm) and at 33 333 cm^{-1} (300 nm). Spectra reported in Figure 13 clearly show how the emission at 20 408 cm^{-1} (490 nm) is preferentially activated by exciting the sample at 39 063 cm^{-1} (256 nm), while the emission at 18 692 cm^{-1} (535 nm) is more active when the zeolite is excited at 33 333 cm^{-1} (300 nm).

The presence of two close peaks at 20 408 cm^{-1} (490 nm) and at 18 692 cm^{-1} (535 nm) is indicative of two slightly different Cu^{+} ions which differ for their local environment. In agreement with the study of Klier *et al.*[110] on Cu^{I}−Y zeolites, the emissions at 20 408 cm^{-1} (490 nm) and at 18 692 cm^{-1} (535 nm) can be assigned to the $3d^{9}4s^{1}(^{3}D_{2}) \rightarrow 3d^{10}(^{1}S_{0})$ electronic transition in isolated cuprous ions in the family of sites **I** and **II**, respectively. Exactly as for the emission spectra, also the excitation band is clearly composed by two distinct bands at 39 063 cm^{-1} (256 nm) and 33 333 cm^{-1} (300 nm), which are also tentatively assigned to $3d^{10}(^{1}S_{0}) \rightarrow 3d^{9}4s^{1}(^{1}D_{2})$ transition of cuprous ions in sites **I** and **II**, respectively. This assignment can be justified as follows: the $3d^{10}(^{1}S_{0}) \rightarrow 3d^{9}4s^{1}(^{1}D_{2})$ transition associated with a remarkable increment of the Cu^{+} ionic radius (from about 0.95 to about 1.6 Å[110]),

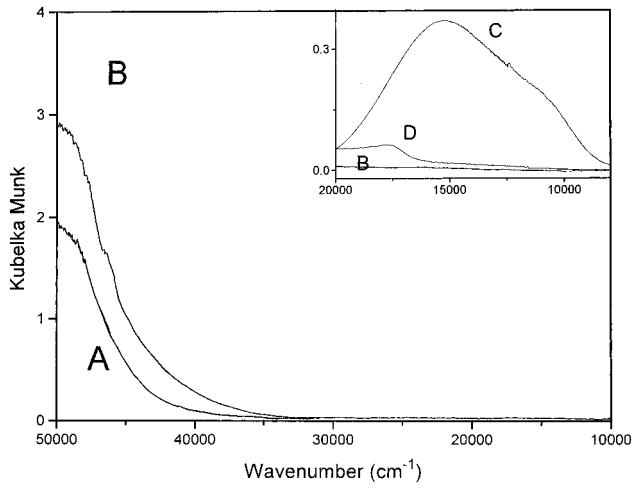

Figure 12. UV−vis−near-IR diffuse reflectance spectra of Cu^{I}-ZSM-5 obtained in the presence of 7 Torr of H_2O (spectrum A) and 10 Torr of NH_3 (spectrum B). The inset represent a magnification in the 20000−8000 cm^{-1} (500−1250 nm) range of spectrum B together with the spectra of a Cu^{II}-ZSM-5 sample (spectrum C) and of a Cu-Y sample exhibiting copper clusters trapped in the supercage,[106,107] both collected under the same experimental conditions. From the inset, the absence in spectrum B of d−d transitions (see spectrum C) and of the Cu^0 metal edge (see spectrum D) is evident.

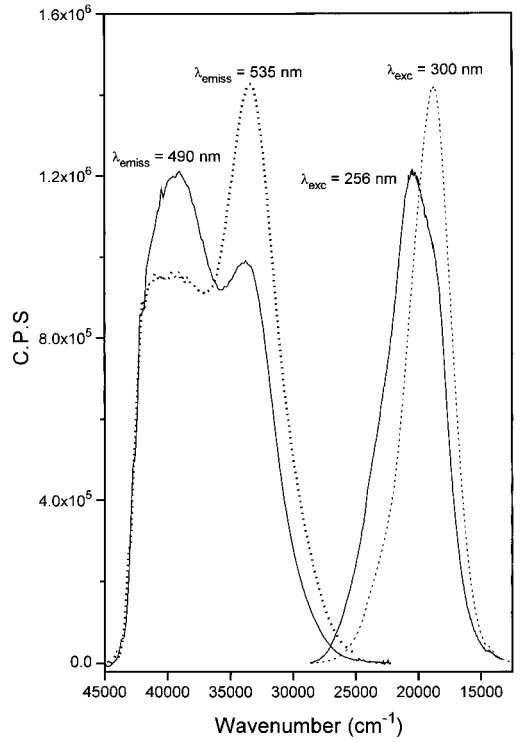

Figure 13. Photoluminescence spectra of Cu^{I}-ZSM-5 collected at *RT* in vacuum conditions. Spectra in the 45000−25000 cm^{-1} (222−400 nm) range represent excitation scans performed with the emission monochromator at 20 408 cm^{-1} (490 nm) and at 18 892 cm^{-1} (535 nm). Spectra in the 12500−25000 cm^{-1} (400−800 nm) range represent emission scans performed with the excitation monochromator at 39 063 cm^{-1} (256 nm) and at 33 333 cm^{-1} (300 nm).

consequently a strong overlapping between the $4s^1$ orbital of the excited Cu^+ ion and the orbitals of the adjacent framework oxygen atoms occurs. The associated strong Coulombic repulsion increases the energy of the transition (which is expected to occur at 26 265 cm^{-1} (381 nm) in the ideal isolated Cu^+ ion[110]). The larger is the coordination number, the greater is the Coulombic repulsion; this is the reason why Cu^+ cations occupying site **I**, being coordinated to three oxygen atoms, are expected to have transitions at higher frequencies than Cu^+ cations located in site **II** which are coordinated to only two oxygen atoms (*vide infra* Figure 15).

These data are in full agreement with the recent findings of Wichterlová *et al.*,[113] who have carried out an accurate photoluminescence study on Cu^{2+}-ZSM-5 (with different Si/Al ratios) prepared using $CuCl_2$ or copper acetate solution and subsequently reduced in H_2 atmosphere to obtain Cu^+ cations. Also the spectra reported in ref 113 show two luminescence bands at 20 830 cm^{-1} (480 nm) and at 18 520 cm^{-1} (540 nm) attributed to two Cu^+ in two different sites. As the increase of the Si/Al ratio favors preferentially the 18 520 cm^{-1} (540 nm) band, the authors of ref 113 distinguish the two sites in terms of Cu^+ adjacent to one or two Al framework atoms, respectively. On the basis of all the techniques reported here, we believe that the difference between the two sites can be also explained in terms of a different first coordination shell of the anchored cation. The two interpretations are not necessarily in conflict because the distribution of Al atoms in the framework is not known. However, the importance of the contribution of Wichterlová *et al.*[113] consists of the established correlation between the integrated intensity of the photoluminescence band at 18 520 cm^{-1} (540 nm) and the catalytical activity. This means that, following our interpretations, the most active sites for the NO decomposition are those showing the highest coordinative unsaturation, *i.e.*, sites **II**.

Kuroda *et al.*,[15] starting from a Cu^{2+}-mordenite prepared from an aqueous solution of ($Cu(NO_3)_2$), obtained Cu^{I}-Cu^{II}-mordenite samples through thermal activation at different temperatures. Samples activated up to 537 K show no photoluminescence emission when excited at 33 300 cm^{-1} (300 nm), while samples activated at higher temperatures show two emissions at 20 800 and 18 700 cm^{-1} (480 and 535 nm). The authors underline that these samples are those that exhibit the sharp 1s → 4p peak at 8983 eV in the XANES spectra. In ref 83 Anpo *et al.*, starting from a Cu^{2+}-ZSM-5 prepared using an aqueous solution of $(Cu(NH_3)_4)_2^{2+}$, obtained Cu^+-ZSM-5 samples through thermal activation and reported three different photoluminescence emissions bands at 23 810 cm^{-1} (420 nm), 21 280 cm^{-1} (470 nm), and 19 420 cm^{-1} (515 nm) with absolute and relative intensities depending upon the activation temperature. The authors of ref 83 attribute the lower energy emission to the radiative $4s\sigma \rightarrow 2d\sigma^*$ deactivation of (Cu^+-Cu^+) dimeric species and the 23 810 cm^{-1} (420 nm) and 21 280 cm^{-1} (470 nm) bands to $3d^94s^1 \rightarrow 3d^{10}$ radiative decay of isolated Cu^+ species having slightly different environments. It must be noticed that, if the presence of (Cu^+-Cu^+) dimeric species is plausible in overexchanged samples prepared through aqueous solution of Cu^{II} ions, their presence in our sample is unlikely because (i) the sample has been prepared through a stoechiometric gas phase reaction with Cu^{I} ions; (ii) the adopted ZSM-5 has a highly siliceous framework, and so the Al atoms are highly isolated; (iii) finally, the absence of any Cu−Cu signal in the EXAFS spectra is not in favor of the relevant presence of (Cu^+-Cu^+) dimers. In relation to this it is worth mentioning that Strome and Klier[111] have observed three different bands at 21 280 cm^{-1} (470 nm), 18 520 cm^{-1} (540 nm), and 17 860 cm^{-1} (560 nm) in the emission spectra of Cu^{I}−Y zeolite and have attributed these emissions to Cu^+ cations located on slightly different oxygen hexagonal rings of the faujasite framework without invoking the presence of dimers.

3.4 EPR Data. While IR and UV−vis techniques are able to detect species present up to some fraction of percent in a diluted sample, the sensitivity of EPR in detecting paramagnetic species is certainly much greater. For this reason, the EPR

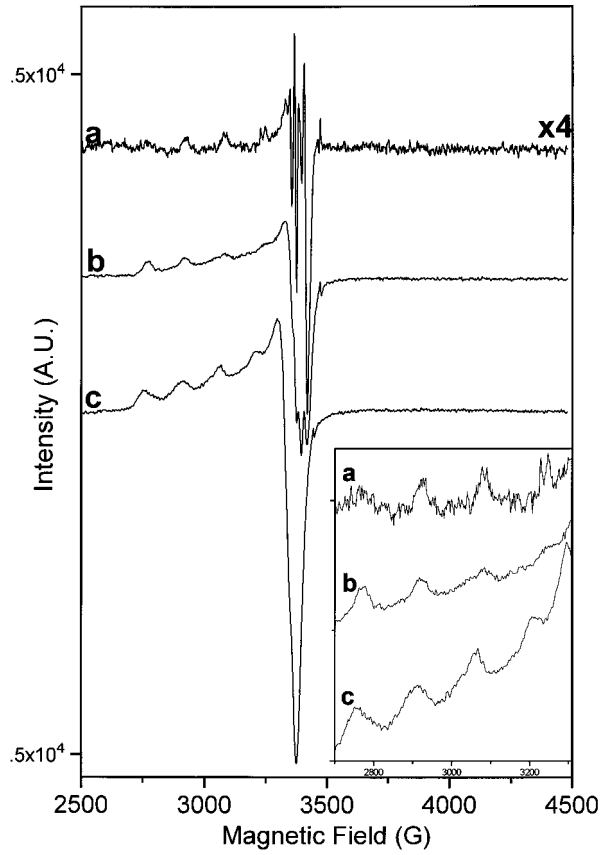

Figure 14. 300 K EPR spectra of the sample in vacuum conditions. (from top to bottom) Virgin sample (spectrum a); after interaction with 6 Torr of NO for 10 min (spectrum b) and subsequent evacuation; after interaction with 6 Torr of NO for 1 h and subsequent evacuation (spectrum c). The inset represents a magnification of the $g_{||}$ signals of spectra a, b, and c (in the inset, the ordinate values have been multiplied by different factors for graphical reasons).

technique has been widely used to characterize Cu^{II} sites in copper-exchanged zeolites.[15,18,43,81,83,109,115−120]

Among all the techniques reported here, only the IR spectroscopy of NO dosed at ≃110−120 K was able to detect a very small quantity of Cu^{II} species (about 1%, see Figure 8 and subsequent discussion); however, this value must be considered for the virgin sample as an upper limit, because part of the Cu^{II} species detected in the experiment reported in Figure 8 could have been generated from the preexisting Cu^{I} ions by oxidation associated with incipient NO decomposition even at ≃110−120 K. We have thus decided to use the EPR technique to further quantify the amount of Cu^{II} species directly on the virgin sample (before contact with NO).

Figure 14 shows the EPR spectra in the following conditions: virgin sample in vacuum (spectrum a); after an interaction with 6 Torr of NO for 10 min and subsequent evacuation (spectrum b); after an interaction with 6 Torr of NO for 1 h and subsequent evacuation (spectrum c).

The spectrum of the virgin sample is typical of isolated Cu^{II} species probably located in only one site. In this case the interference between neighboring Cu^{II} centers can be totally neglected and the spectrum can be fundamentally described in terms of an axial spectrum with $g_1 \equiv g_{||}$ and $g_2 = g_3 \equiv g_{\perp}$, whose g components are split into quartets due to the hyperfine interaction between the unpaired electron and the copper nucleus (having both ^{63}Cu and ^{65}Cu nuclei with a nuclear spin of $^{3}/_{2}$).[81,115] The weakness of the signal reported in the spectrum is evident, the intensity of the $g_{||}$ and $g_{\perp}$ signals being only 3 and 20 times, respectively, the instrumental noise level. The spin-Hamiltonian parameters of Cu^{2+} ions are: $g_{||} \simeq 2.30$, $g_{\perp} \simeq 1.94$, $A_{||} \simeq 155$ G, and $A_{\perp} \simeq 20$ G, values very close to those reported by Giamello *et al.*[81] for a Cu^{2+}-ZSM-5 thermally reduced at 873 K (species labeled as A in that work).

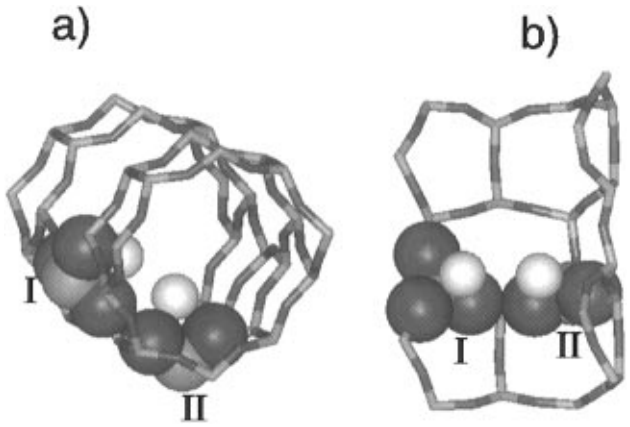

Figure 15. Computer graphic pictures showing the 10-membered rings composing the ZSM-5 linear channel and evidencing the two Cu^{+} locations compatible with the observed EXAFS, IR, and UV−vis data. Cu^{+} cations (white spheres) and corresponding nearest-neighbor framework oxygens (black spheres) bridged with the same Al atom (gray spheres) are evidenced. Parts a and b report two different views.

After an interaction with 6 Torr of NO for 10 min and subsequent evacuation (spectrum b), the EPR signal has increased by a factor of 17; Cu^{II} ions still remain isolated species, probably located in two slightly different sites (as documented by the shoulder appearing in each component of $g_{||}$; see inset). The hyperfine lines on the perpendicular component are still visible, although less resolved than in spectrum a. After an interaction with the same NO pressure for 60 min and subsequent evacuation (spectrum c), the EPR signal has increased by a factor of 30. Under these conditions Cu^{II} ions cannot be considered anymore as isolated species (this means that their magnetic interaction cannot be neglected). The high density of Cu^{II} ions in the sample measured after 1 h of contact with NO is demonstrated not only by the intensity increase of the $g_{\perp}$ signal in spectrum c, but also by the total loss of resolution in the perpendicular component, which is a typical effect of dipolar interactions between Cu^{II} sites.[81]

In conclusion, from the IR experiments reported in Figures 9−11 we have learned that after about 1 h interaction with NO atmosphere at *RT*, about 28% of the original Cu^{I} counterions have been oxidized into Cu^{II} species. On this basis, the present EPR data, where we have observed an increment of a factor of 30 of the Cu^{II} sites after the same treatement, allows the conclusion that the fraction of Cu^{II} cations present in the virgin sample is about 0.9% (*i.e.*, 28/30) of the total copper species present in the Cu^{I}-ZSM-5.

3.5 Location of Cu^{I} in Cu^{I}-ZSM-5. ZSM-5 is a silicon-rich zeolite having a MFI type structure[121] where the Al atoms are randomly distributed in the framework.[122] Due to the small Al content, the zeolite framework has essentially a covalent character and only the oxygen atoms linked to an aluminium carry a significant negative charge. For electrostatic reasons, Cu^{+} cations will thus find their location by maximizing the coordination to these oxygens.[123]

Computer graphic facilities,[37] enable careful investigation of the T centers forming the channels walls. We have identified two different families of T tetrahedra; the first exhibiting three oxygens exposed on the channel and the second showing only two oxygens exposed on the channel. If the TO_4 tetrahedron contains Al, then the oxygens are negatively charged and become the ideal location sites for counterions; see Figure 15.

We can consequently speak about two families of sites. In the first family, already indicated as family **I**, the Cu^I ion is surrounded by three equivalent nearest neighbor framework oxygens, at about 2 Å, which are all exposed in the channel, defining an equilateral triangle having a side of 2.6 Å (see Figure 15). In the second family, already labeled as family **II**, the Cu^I ion is surrounded by only two equivalent nearest neighbor framework oxygens at about 2 Å, both exposed in the channel and by a third, more internally located, at about 3 Å (see Figure 15).

This situation is fully compatible with the reported EXAFS results (see Table 1), which report in vacuum conditions 2.5 ± 0.3 oxygens at 2.00 ± 0.02 Å. The value 2.5 ± 0.3 for the coordination number is thus probably the results of signals coming from Cu^I ions nearly equidistributed in families **I** and **II**. In fact, copper ions located in family **I** would give rise to $N = 3.0$, while copper species located in family **II** would yield $N = 2.0$, the third oxygen at about 3 Å playing a negligible role in a one-shell fit. Moreover, this picture is able to explain why only one family of sites is able to coordinate up to three CO molecules at $\simeq$110−120 K and why both emission and excitation photoluminescence spectra exhibit two distinct components.

4 Conclusions

In this work we have combined the characterization capabilities of IR and UV−vis spectroscopies with the atomic selectivity of XAFS to investigate the local environment of Cu^I in a model Cu^I-ZSM-5 catalyst prepared through a gas phase reaction with CuCl.[20,21] The XANES part of the X-ray absorption spectrum indicates that the copper species are mainly in an oxidation state of I. This datum is quantitatively supported by UV−vis data and by IR spectroscopy of adsorbed CO, N_2, and NO. From the IR and UV−vis results we are able to conclude that the Cu^{II} concentration was not higher than 1%. Comparison between the EPR spectra measured before and after interaction with NO definitely confirms that the amount of Cu^{II} species in the virgin sample is below 1%. The analysis of the EXAFS part of the X-ray absorption spectrum also discards the presence of copper dimeric or clustered species and ensures that unreacted CuCl molecules are not present in the Cu environment; this conclusion is also strongly supported by both IR and UV−vis spectroscopies. All the presented results confirm that it is possible to obtain, by means of an adequate preparation procedures,[20,21] monodispersed Cu^I ions in ZSM-5 zeolite. The combined use of EXAFS, IR, photoluminescence, and computer graphic simulations allows the inference that Cu^I ions in Cu^I-ZSM-5 are nearly (at *RT*) equidistributed in two families of sites.

Acknowledgment. We are indebted to E. Giamello and C. Paganini for EPR measurements and related fruitful discussion, to F. Villaine and H. Sonneville for providing helpful and important assistance during the EXAFS experiments at LURE, and to G. Petrini, F. Genoni, and G. Leofanti for the stimulating collaboration. S.B. and F.G. gratefully acknowledge the financial support from LURE for their trip and their stay in Orsay. C.L. is indebted to M. L. Vighi Mileto, R. Rossetto, and all his colleagues at XI L.S.S. (Giordano Bruno) of Turin for their continuous encouragement. The constructive suggestions of both referee are also acknowledged.

Note Added in Proof. An improvement of the IR experimental conditions has allowed to collect spectra at about 80−90 K: at this temperature the transformation of $Cu^I(CO)_2 \xrightarrow{CO} Cu^I(CO)_3$ involves the totality of Cu^I ions.[124] This means that under appropriate conditions a third molecule of CO can be included in the coordination sphere of Cu^I in site **I**.

References and Notes

(1) Iwamoto, M.; Yokoo, S.; Sakai, K.; Kagawa, S. *J. Chem. Soc., Faraday Trans. 1* **1981**, *77*, 1629. Iwamoto, M.; Furukawa, H.; Mine, Y.; Umera, F.; Mikuriya S. Kagawa, S. *J. Chem. Soc., Chem. Commun.* **1986**, 1272. Iwamoto, M.; Yahiro, H.; Mine, Y.; Kagawa, S. *Chem. Lett.* **1989**, 213. Iwamoto, M.; Yahiro, H.; Kutsuno, T.; Bunyu, S.; Kagawa, S. *Bull. Chem. Soc. Jpn.* **1989**, *62*, 583. Iwamoto, M.; Hamada, H. *Catal. Today* **1991**, *10*, 57. Iwamoto, M. *Stud. Surf. Sci. Catal.* **1990**, *54*, 121. Iwamoto, M.; Yahiro, H.; Sundo, S.; Yu-u, Y.; Mizuno, N. *Appl. Catal.* **1991**, *69*, L15.

(2) Li, Y.; Hall, W. K. *J. Phys. Chem.* **1990**, *94*, 6145.

(3) Shelef, M. *Chem. Rev.* **1995**, *95*, 209 and references therein.

(4) Spoto, G.; Bordiga, S.; Ricchiardi, G.; Scarano, D.; Zecchina, A.; Geobaldo, F. *J. Chem. Soc., Faraday Trans.* **1995**, *91*, 3285.

(5) Parillo, F. J.; Fortney, P.; Gorte, R. J. *J. Catal.* **1995**, *153*, 190. Cho, B. K. *Ibid.* **1995**, *155*, 184.

(6) Komatsu, T.; Ogawa, T.; Yashima, T. *J. Phys. Chem.* **1995**, *99*, 13053. Dědeček, J.; Sobal'k Z.; Tvaružková, Z.; Wichterlová, B. *Ibid.* **1995**, *99*, 16327. Trout, B. L.; Chakraborty, A. K.; Bell, A. T. *Ibid.* **1996**, *100*, 4173. Schneider, W. F.; Hass, K. C.; Ramprasad, R.; Adams, J. B. *Ibid.* **1996**, *100*, 6032. Schneider, W. F.; Hass, K. C. *Ibid.* **1996**, *100*, 9292. Yokomichi, Y.; Yamabe, T.; Ohtsuka, H.; Kakumoto, T. *Ibid.* **1996**, *100*, 14424. Trout, B. L.; Chakraborty, A. K.; Bell, A. T. *Ibid.* **1996**, *100*, 17582.

(7) Yokomichi, Y.; Othsuka, H.; Tabata, T.; Okada, O.; Yokoi, Y.; Ishikava, H.; Yamaguchi, R.; Matsui, H.; Tachibana, A.; Yamabe, T. *Catal. Today* **1995**, *23*, 431. Tabata, T.; Othsuka, H.; Kokitsu, M.; Okada, O. *Bull. Chem. Soc. Jpn.* **1995**, *68*, 1905.

(8) Ciambelli, P.; Corbo, P.; Gambino, M.; Migliardini, F.; Minelli, G.; Moretti, C.; Porta, P. *Stud. Surf. Sci. Catal.* **1995**, *97*, 295. Kapteijn, F.; Mul, G.; Marbán, G.; Mirasol, J. F.-; Mouijn, J. A. *Ibid.* **1996**, *101*, 641.

(9) Centi, G.; Perathoner, S. *Appl. Catal. A* **1995**, *132*, 179. Sasaki, M.; Hamada, H.; Kintaichi, Y.; Ito, T. *Ibid.* **1995**, *132*, 261.

(10) Wang, W.; Hwang, S.-J. *Appl. Catal. B* **1995**, *5*, 187. Smits, R. H. H.; Iwasawa, Y. *Ibid.* **1995**, *6*, L201. Panayotov, D.; Dimitrov, L.; Khristova, M.; Petrov, L.; Mehandjiev, D. *Ibid.* **1995**, *6*, 61. Tanabe, T.; Iijima, T.; Koiwai, A.; Mizuno, J.; Yokota, K.; Isogai, A. *Ibid.* **1995**, *6*, 145. Coq, B.; Tachon, D.; Figueras, F.; Mabilon, G.; Prigent, M. *Ibid.* **1995**, *6*, 271. Hoost, T. E.; Laframboise, K. A.; Otto, K. *Ibid.* **1995**, *7*, 79. Guyon, M.; Le Chanu, V.; Gilot, P.; Kessler, H.; Prado, G. *Ibid.* **1996**, *8*, 183. Pirone, R.; Ciambelli, P.; Moretti, G.; Russo, G. *Ibid.* **1996**, *8*, 197. Ciambelli, P.; Garufi, E.; Pirone, R.; Russo G.; Santagata, F. *Ibid.* **1996**, *8*, 333. Hayes, N. W.; Joyner, R. W.; Shpiro, E. S. *Ibid.* **1996**, *8*, 343. Turek, T. *Ibid.* **1996**, *9*, 201. Beutel, T.; Adelman, B. J.; Sachtler, W. M. H. *Ibid.* **1996**, *9*, L1. Adams, K. M.; Cavataio, J. V.; Hammerle R. H. *Ibid.* **1996**, *10*, 157.

(11) Ciambelli, P.; Corbo, P.; Gambino, M.; Migliardini, F.; Minelli, G.; Moretti, C.; Porta, P. *Catal. Today* **1995**, *26*, 33. Walker, A. P. *Ibid.* **1995**, *26*, 107. Radtke, F.; Koppel, R. A.; Baiker, A. *Ibid.* **1995**, *26*, 159. Bethke, K. A.; Kung, M. C.; Yang, B.; Shah, M.; Alt, D.; Li, C.; Kung, H. H. *Ibid.* **1995**, *26*, 169. Matsumoto, S. *Ibid.* **1996**, *29*, 43. Centi, G.; Perathoner S. *Ibid.* **1996**, *29*, 117.

(12) Oka, H.; Okada, T.; Hori, K. *J. Mol. Catal. A* **1996**, *109*, 51.

(13) Kucherov, A. V.; Slovetskaya, K. I.; Goryaschenko, S. S.; Aleshin, E. G.; Slinkin, A. A. *Microporous Mater.* **1996**, *7*, 27.

(14) Kharas, K. C. C.; Liu, D.-J.; Robota, H. J. *Catal. Today* **1995**, *26*, 129.

(15) Kuroda, Y.; Yoshikawa, Y.; Konno, S.; Hamano, H.; Maeda, H.; Kumashiro, R.; Nagao, M. *J. Phys. Chem.* **1995**, *99*, 10621.

(16) Tanabe, S.; Matsumoto, H. *Chem. Lett.* **1989**, 539; *J. Chem. Soc., Chem. Commun.* **1989**, 875; *Bull. Chem. Soc. Jpn.* **1990**, *63*, 192.

(17) Iwamoto, M.; Yahiro, H.; Tanada, K.; Mizumo, N.; Mine, Y.; Kagawa, S. *J. Phys. Chem.* **1991**, *95*, 3727.

(18) Grünert, W.; Hayes, N. W.; Joyner, R. W.; Shpiro, E. S.; Rafiq, M.; Siddiqui, H.; Baeva, G. N. *J. Phys. Chem.* **1994**, *98*, 10832.

(19) Hamada, H.; Matsubayashi, N.; Shimada, H.; Kintaichi, Y.; Ito, T.; Nishijima, A. *Catal. Lett.* **1990**, *5*, 189.

(20) Spoto, G.; Bordiga, S.; Scarano, D.; Zecchina, A. *Catal. Lett.* **1992**, *13*, 39.

(21) Spoto, G.; Zecchina, A.; Bordiga, S.; Ricchiardi, G.; Martra, G.; Leofanti, G.; Petrini, G. *Appl. Catal. B* **1994**, *3*, 151.

(22) Li, Y.; Hall, W. K. *J. Catal.* **1991**, *129*, 202.

(23) Stern, E. A. *Phys. Rev. B* **1974**, *10*, 3027. Teo, B. K.; Joy, D. C. *EXAFS Spectroscopy: Techniques and Applications*; Plenum: New-York, 1981. Lee, P. A.; Citrin, P. H.; Eisenberger, P.; Kincaid, M. *Rev. Mod. Phys.* **1981**, *53*, 769. Hayes, T. M.; Boyce, J. B. *Solid State Phys.* **1982**, *37*, 173. Stern, E. A. in *X-Ray Absorption*; Koningsberger, D. C., Prins, R., Eds.; Wiley & Sons: New York, 1988; p 3.

(24) Zecchina, A.; Bordiga, S.; Spoto, G.; Scarano, D.; Petrini, G.; Leofanti, G.; Padovan, M.; Otero Areán, C. *J. Chem. Soc., Faraday Trans.* **1992**, *88*, 2959.

(25) Bordiga, S.; Coluccia, S.; Lamberti, C.; Marchese, L.; Zecchina, A.; Boscherini, F.; Buffa, F.; Genoni, F.; Leofanti, G.; Petrini, G.; Vlaic, G. *J. Phys. Chem.* **1994**, *98*, 4125.

(26) Bordiga, S.; Boscherini, F.; Coluccia, S.; Genoni, F.; Lamberti, C.; Leofanti, G.; Marchese, L.; Petrini, G.; Vlaic, G.; Zecchina, A. *Catal. Lett.* **1994**, *26*, 195.

(27) Bordiga, S.; Geobaldo, F.; Lamberti, C.; Zecchina, A.; Boscherini, F.; Genoni, F.; Leofanti, G.; Petrini, G.; Padovan, M.; Geremia, S.; Vlaic, G. *Nucl. Instrum. Methods Phys. Res. B* **1995**, *97*, 23.

(28) Bordiga, S.; Buzzoni, R.; Geobaldo, F.; Lamberti, C.; Giamello, E.; Zecchina, A.; Leofanti, G.; Petrini, G.; Tozzola, G.; Vlaic, G. *J. Catal.* **1996**, *158*, 486.

(29) LURE, Guide Technique Postes Experimentaux 1992, Ligne D42, p 63.

(30) Zecchina, A.; Bordiga, S.; Lamberti, C.; Petrini, G.; Leofanti, G.; Genoni, F.; Vlaic, G.; LURE, proposal no. CK 007, 1994.

(31) Lytle, F. W.; Sayers, D. E.; Stern, E. A. *Physica B* **1989**, *158*, 701.

(32) Lengeler, B.; Eisenberger, P. *Phys. Rev. B* **1980**, *21*, 4507.

(33) Michalowicz, A. Ph.D. Thesis, Université Paris Val de Marne, 1990. Michalowicz, A. *Structures fines d'absorption an Chimie*; Verdaguer, M., Michalowicz, A., Dexpert, H., Eds.; Ecole du CNRS: Garchy, 1989. Michalowicz, A. In *Logicels pour la Chimie*; Societé Francaise de Chimie: Paris, 1991; p 102.

(34) James, F.; Roos, M. *Comput. Phys. Commun.* **1975**, *10*, 343.

(35) Dossi, C.; Psaro, R.; Bartsch, A.; Fusi, A.; Sordelli, L.; Ugo, R.; Bellatreccia, M.; Zanoni, R.; Vlaic, G. *J. Catal.* **1994**, *145*, 377.

(36) Joyner, R. W.; Martin, K. J.; Meehan, P. *J. Phys. C* **1987**, *20*, 4005.

(37) Insight II, version 3.0.0, Biosym/MSI Technology Inc., San Diego, CA, October 1995.

(38) Liu, D.-J.; Robota, H. J. *Catal. Lett.* **1993**, *21*, 291; *Appl. Catal. B* **1994**, *4*, 155.

(39) Karas, K. C. C. *Appl. Catal. B* **1993**, *2*, 207.

(40) Beutel, T.; Sárkány. J.; Lei, G.-D.; Yan, J. Y.; Sachtler, W. M. H. *J. Phys. Chem.* **1996**, *100*, 845.

(41) Yamashita, H.; Matsuoka, M.; Tsuji, K.; Shioya, Y.; Anpo, M.; Che, M. *J. Phys. Chem.* **1996**, *100*, 397.

(42) Kuroda, Y.; Maeda, H.; Moriwaki, H.; Bamba, N.; Morimoto, T. *Physica B* **1989**, *158*, 185.

(43) Kuroda, Y.; Kotani, A.; Maeda, H.; Moriwaki, H.; Morimato, T.; Nagao, M. *J. Chem. Soc., Faraday Trans.* **1992**, *88*, 1583.

(44) Choi, E. Y.; Nam, I.-S.; Kim, Y. G.; Chung, J. S. Lee, J. S. *J. Mol. Catal.* **1991**, *69*, 247.

(45) Tanabe, S.; Matsumoto, H. *J. Phys. Chem.* **1990**, *94*, 4207.

(46) Antonioli, G.; Vlaic, G.; Nardin, G.; Randaccio, L. *J. Chem. Soc., Dalton Trans.* **1990**, 943; *Conf. Proc. Ital. Phys. Soc.* **1990**, *25*, 579.

(47) Lamberti, C.; Salvalaggio, M.; Bordiga, S.; Geobaldo, F.; Spoto, G.; Zecchina, A.; Vlaic V.; Bellatreccia B. Presented at the 9th International Conference on XAFS, Grenoble (F), 26−30 Aug 1996; *J. Phys. IV*, in press.

(48) Tranquada, J. M.; Heald, S. M.; Moodenbaugh, A. R. *Phys. Rev. B* **1987**, *36*, 5263.

(49) Brown, J. M.; Powers, L.; Kincaid, B.; Larrabee, J. A.; Spirp, T. G. *J. Am. Chem. Soc.* **1980**, *102*, 4210.

(50) LuBien, C. D.; Winkler, M. E.; Thamann, T. J.; Scott, R. A.; Co, M. S.; Hodgson, K. O.; Solomon, E. I. *J. Am. Chem. Soc.* **1981**, *103*, 7014.

(51) Kau, L. S.; Spira-Solomon, D. J.; Penner-Hahn, J. E.; Hodgson, K. O.; Solomon, E. I. *J. Am. Chem. Soc.* **1987**, *109*, 6433. Kau, L. S.; Hodgson, K. O.; Solomon, E. I. *Ibid.* **1989**, *111*, 7103.

(52) Blackburn, N. J.; Strange, R. W.; Reedijk, J.; Volbeda, A.; Farooq, A.; Karlin, A.; Zubieta, J. *Inorg. Chem.* **1989**, *28*, 1349. Blackburn, N. J.; Hasnain, S. S.; Pettigrill, T. M.; Strange, R. W. *J. Biol. Chem.* **1991**, *266*, 23120. Reedy, B. J.; Blackburn, N. J. *J. Am. Chem. Soc.* **1994**, *116*, 1924.

(53) Smith, T. A.; Penner-Hahn, J. E.; Hodgson, K. O.; Berding, M. A.; Doniach, S. *Springer Proc. Phys.* **1984**, *2*, 58.

(54) Lamble, G.; Moen, A.; Nicholson, D. G. *J. Chem. Soc., Faraday Trans.* **1994**, *90*, 2211; *Ibid.* **1995**, *91*, 3189. Moen, A.; Nicholson, D. G. *Ibid.* **1995**, *91*, 3529.

(55) Hahn, J. E.; Scott, R. A.; Hodgson, K. O.; Doniach, S.; Desjardins, S. R.; Solomon, E. I.; *Chem. Phys. Lett.* **1982**, *88*, 595. Nomura, M.; Kazusaka, A.; Kakuta, N.; Ukisu, Y.; Miyahara, K. *Ibid.* **1985**, *122*, 538. Bianconi, A. in *X-Ray Absorption*; Koningsberger, D. C.; Prins, R., Eds.; Wiley & Sons: New York, 1988; p 573.

(56) Blair, R. A.; Goddard, W. A. *Phys. Rev. B* **1980**, *22*, 2767. Kosugi, N.; Yokoyama, T.; Asakuna, K.; Kuroda, H. *Chem. Phys.* **1984**, *91*, 249; *Springer Proc. Phys.* **1984**, *2*, 55.

(57) Kuroda, Y.; Konno, S.; Morimoto, K.; Yoshikawa, Y. *J. Chem. Soc., Chem. Commun.* **1993**, 18.

(58) Hunag, Y. *J. Am. Chem. Soc.* **1973**, *95*, 6636; *J. Catal.* **1973**, *30*, 187.

(59) Lee, P. A.; Beni, G. *Phys. Rev. B* **1977**, *15*, 2862.

(60) Sayers, D. E.; Bunker, B. A. In *X-Ray Absorption*; Koningsberger, D. C., Prins, R., Eds.; Wiley & Sons: New York, 1988; p 211.

(61) Ugliengo, P.; Saunders, V. P.; Garrone, E. *J. Phys. Chem.* **1989**, *93*, 5210. Ferrari, A. M.; Ugliengo, P.; Garrone, E. *J. Chem. Phys.* **1996**, *105*, 4129.

(62) Zecchina, A.; Bordiga, S.; Lamberti, C.; Spoto, G.; Carnelli, L.; Otero Areán, C. *J. Phys. Chem.* **1994**, *98*, 9577. Bordiga, S.; Lamberti, C.; Geobaldo, F.; Zecchina, A.; Turnes Palomino, G.; Otero Areán, C. *Langmuir* **1995**, *11*, 527. Lamberti, C.; Bordiga, S.; Geobaldo, F.; Zecchina, A.; Otero Areán, C. *J. Chem. Phys.* **1995**, *103*, 3158.

(63) Bordiga, S.; Garrone, E.; Lamberti, C.; Zecchina, A.; Otero Areán, C.; Kazansky, V. B.; Kustov, L. M.; *J. Chem. Soc., Faraday Trans.* **1994**, *90*, 3367.

(64) Katoh, M.; Yamazaki, T.; Ozawa, S. *Bull. Chem. Soc. Jpn.* **1994**, *67*, 1246.

(65) Lee, P. A.; Pendry, J. B. *Phys. Rev. B* **1975**, *11*, 2795. Beni, G.; Lee, P. A.; Paltzman, P. M. *Phys. Rev. B* **1976**, *13*, 5170. Teo, B. K. *J. Am. Chem. Soc.* **1981**, *103*, 3990.

(66) Filipponi, A.; Di Cicco, A.; Natoli, C. R. *Phys. Rev. B* **1995**, *52*, 15122 and references therein. Fonda, L. *J. Phys.: Condens. Matter* **1992**, *4*, 8269 and references therein.

(67) It is in fact well-known that when a photoelectron is emitted by an excited atom *O* (Cu in our case) surrounded by two adjacent atoms *i* and *j* (which are the atoms of the carbon monoxide in our case) the corresponding EXAFS signal is generated not only by the so-called two-body paths which, at the lower order, are from *O* to *i* and back to *O* and from *O* to *j* and back to *O* but also from three bodies paths like that from *O* to *i* to *j* and back to *O*. The first two contributions are those considered when the single-scattering approach is adopted, while the third is one of the additional paths that must be considered when a multiple-scattering (MS) approach is undertaken. Due to the fact that the photoelectron has a short mean-free path, the single-scattering contributions are normally (but not always) predominant and analyses performed in this frame represent, normally (but not always) an acceptable approximation.[68] This is certainly true when only the first shell contributes significantly to the experimental EXAFS signal, like the case of the zeolite in vacuum (see Figure 4 and related discussion); however, when more shells contribute to the experimental EXAFS signal in a significant way, a more cautious approach is needed. In such cases we believe that a single-scattering analysis can be safely performed only if, *a priori*, an evaluation of the MS contributions has proven that corresponding signals are negligible if compared to the single-scattering contributions. This is certainly not the case when *O*, *i*, and *j* atoms exhibit a linear geometry like *i*−*O*−*j*, or *O*−*i*−*j* (which is what happens when CO is dosed on the zeolite, forming Cu−C−O linear adducts), where the contributions of the MS paths are strongly enhanced and cannot be neglected anymore.[65] On the other hand, the strong importance of MS contributions in several metal carbonyl compounds has been already experimentally evidenced; see, *e.g.*, ref 69.

(68) Brunker, G.; Stern, E. A. *Phys. Rev. Lett.* **1984**, *52*, 1990. Bouldin, C. E.; Brunker, G.; McKeown, D. A.; Forman, R. A.; Ritter, J. J. *Phys. Rev. B* **1988**, *38*, 10816.

(69) Pettifer, R. F. *Stud. Surf. Sci. Catal.* **1986**, *29*, 254. Gurman, S. J.; Binsted, N.; Ross, I. *J. Phys. C* **1986**, *38*, 1845. Binsted, N.; Cook, S. L.; Evans, J.; Graevens, G. N.; Price, R. J. *J. Am. Chem. Soc.* **1987**, *109*, 3669. Filipponi, A.; Di Cicco, A.; Zanoni, R.; Bellatreccia, M.; Sessa, V.; Dossi, C.; Psaro, R. *Chem. Phys. Lett.* **1991**, *184*, 485.

(70) Filipponi, A.; Di Cicco, A.; Tyson, T. A.; Natoli, C. R. *Solid State Commun.* **1991**, *78*, 265. Filipponi, A.; Di Cicco, A. *Syncrotron Radiat. News* **1993**, *6*, 13. Di Cicco, A. *Physica B* **1995**, *208/209*, 125. Filipponi, A.; Di Cicco, A. *Phys. Rev. B* **1995**, *52*, 15135.

(71) Zabinsky, S. I.; Rehr, J. J.; Ankudinov, A.; Albers, R. C.; Eller, M. J. *Phys. Rev. B* **1995**, *52*, 2995. Rehr, J. J.; Albers, R. C.; Zabinsky, S. I. *Phys. Rev. Lett.* **1992**, *69*, 3397.

(72) Binsted, N.; Cook, S. L.; Evans, J.; Greaves, G. N.; Price, R. J. *J. Am. Chem. Soc.* **1987**, *109*, 3669. Binsted, N.; Campbell, J. W.; Gurman, S. J.; Stephenson, P. C. *EXCALIB*, *EXBACK*, and *EXCURV 92*; Daresbury Laboratory: Warrington, 1992.

(73) Lamberti, C.; *et al.* Manuscript in preparation.

(74) Ward, J. W. In *Zeolite Chemistry and Catalysis*; Rabo, J. A., Ed.; ACS Monograph Series 171; American Chemical Society: Washington, DC, 1976; p 118 and references therein.

(75) Zecchina, A.; Otero Areán, C. *Chem. Soc. Rev.* **1996**, *25*, 187.

(76) Márquez-Alvarez, C.; McDougall, G. S.; Guerrero-Ruiz, A.; Rodríguez, I. *Appl. Surf. Sci.* **1994**, *78*, 477.

(77) Aylor, A. W.; Larsen, S. C.; Reimer, J. A.; Bell, A. T. *J. Catal.* **1995**, *157*, 592.

(78) Sárkány. J.; d'Itri, J. L.; Sachtler, W. M. H. *Catal. Lett.* **1992**, *16*, 241. Sárkány. J.; Sachtler, W. M. H. *Zeolites* **1994**, *14*, 7.

(79) Iwamoto, M.; Yahiro, H.; Mizumo, N.; Zhang, W.-X.; Mine, Y.; Furukawa, H.; Kagawa, S. *J. Phys. Chem.* **1992**, *96*, 9360.

(80) Itho, Y.; Nishiyama, S.; Tsuruya, S.; Masai, M. *J. Phys. Chem.* **1994**, *98*, 960.

(81) Giamello, E.; Murphy, D.; Magnacca, G.; Morterra, C.; Shioya, Y.; Nomura, T.; Anpo, M. *J. Catal.* **1992**, *136*, 510.

(82) Petunchi, G. O.; Marcelin, F.; Hall, W. K. *J. Phys. Chem.* **1992**, *96*, 9967. Valyon, J.; Hall, W. K. *Stud. Surf. Sci. Catal.* **1993**, *75B*, 1338.

Valyon, J.; Hall, W. K. *J. Phys. Chem.* **1993**, *97*, 1204, 7054. Jang, H.-J.; Hall, W. K.; d'Itri, J. L. *J. Phys. Chem.* **1996**, *100*, 9416.

(83) Anpo, M.; Matsuoka, M.; Shioya, Y.; Yamashita, H.; Giamello, E.; Morterra, C.; Che. M.; Patterson, H. H.; Webber, S.; Ouellette, S.; Fox, M. A. *J. Phys. Chem* **1994**, *98*, 5744.

(84) Cheung, T.; Bhargava, S. K.; Hobday, M.; Foger, K. *J. Catal.* **1996**, *158*, 301.

(85) Adelman, B. J.; Beutel, T.; Lei, G.-D.; Sachtler, W. M. H. *J. Catal.* **1996**, *158*, 327.

(86) King, S. T. *J. Catal.* **1996**, *161*, 530.

(87) Matyshak, V. A.; Baron, S. L.; Ukharskii, A. A.; Il'ichev, A. N.; Sadycov, V. A.; Korchak, V. N. *Katal. Katal.* **1996**, *37*, 585.

(88) Ewing, G. E. *J. Chem. Phys.* **1962**, *37*, 2250.

(89) Cox, D. F.; Schulz, K. H. *Surf. Sci.* **1991**, *249*, 138.

(90) Salomon, E. I.; Jones, P. M.; May, J. A. *Chem. Rev.* **1993**, *93*, 2623.

(91) García, M. F.; Conesa, J. C.; Illas, F. *Surf. Sci.* **1996**, *349*, 207.

(92) Rack, J. J,; Webb, J. D.; Strauss, S. H. *Inorg. Chem.* **1996**, *35*, 277.

(93) Lamberti, C.; Bordiga, S.; Cerrato, G.; Morterra, C.; Scarano, D.; Spoto, G.; Zecchina, A. *Comput. Phys. Commun.* **1993**, *74*, 119.

(94) Lamberti, C.; Morterra, C.; Bordiga, S.; Cerrato, G.; Scarano, D. *Vib. Spectrosc.* **1993**, *4* 273.

(95) Huber, H.; Künding E. P.; Moskovits, M.; Ozin, G. A. *J. Am. Chem. Soc.* **1973**, *95*, 332. Ozin, G. A.; Vander Voet, A. *Can. J. Chem.* **1973**, *51*, 3332. Plitt, H. S.; Schnöckel, Bär, M.; Ahlrichs, R. *Z. Anorg. Allg. Chem.* **1992**, *607*, 45.

(96) Garrone, E. Bolis, V.; Fubini, B.; Morterra, C.; *Langmuir* **1989**, *5*, 892. Bolis, V.; Morterra, C.; Fubini, B.; Ugliengo, P.; Garrone, E. *Ibid.* **1993**, *9*, 1521.

(97) Bordiga, S.; Escalona Platero, E.; Otero Areán, C.; Lamberti, C.; Zecchina, A. *J. Catal.* **1992**, *137*, 179. Bordiga, S.; Scarano, D.; Spoto, G.; Zecchina, A.; Lamberti, C.; Otero Areán, C. *Vib. Spectrosc.* **1993**, *5*, 69.

(98) Geobaldo, F.; Lamberti, C.; Ricchiardi, G.; Bordiga, S.; Zecchina, A.; Turnes Palomino G.; Otero Areán, C. *J. Phys. Chem.* **1995**, *99*, 11167.

(99) Nakamoto, K. *Infrared and Raman spectra of inorganic and coordination compounds*; John Wiley: New York, 1986.

(100) It must be considered that, moreover even at such a low temperature (≃110−120 K), a weak $Cu^{+} \rightarrow Cu^{2+}$ oxidation through NO cannot be totally excluded; this means that the amount of Cu^{II} sites observed during the experiment reported in Figure 8 must be considered as an upper limit for the Cu^{II} concentration on the virgin sample. A more precise extimation will be given after the discussion of the EPR data; *vide infra* section 3.4.

(101) Dinerman, C. E.; Ewing, G. E. *J. Chem. Phys.* **1970**, *53*, 626. Kometer, R.; Legay, F.; Legay-Sommaire, N.; Schwentner, N. *Ibid.* **1994**, *100*, 8737.

(102) In a separated experiment, not shown for sake of brevity, we have dosed the virgin Cu^{I}-ZSM-5 sample N_2O at ≃110−120 K. We have observed that the so-formed $Cu^{I}(N_2O)$ adducts give rise to an IR absorption at 2293 cm^{-1} and are easily evacuated upon outgassing at ≃110−120 K.

(103) Laane, J.; Ohlsen, J. R. *Prog. Inorg. Chem.* **1980**, *27*, 645 and references therein.

(104) Kasai, P. H.; Bishop, R. J. *J. Am. Chem. Soc.* **1972**, *94*, 5560. Kasai, P. H.; Bishop, R. J. In *Zeolite Chemistry and Catalysis*; Rabo, J. A., Ed.; ACS Monograph Series 171; American Chemical Society: Washington, DC, 1976; p 350 and references therein.

(105) Ferrandi, G.; Muralidharan, S. *Coord. Chem. Rev.* **1981**, *36*, 45.

(106) Details on the preparation and on the characterization of Cu-Y sample can be found in ref 107.

(107) D'Acapito, F.; Turnes Palomino, G.; Lamberti, C.; Bordiga, S.; Pazé, C.; Spoto, S.; Zecchina, A. Presented at the 9th International Conference on XAFS, Grenoble (F), 26−30 Aug 1996; *J. Phys. IV*, in press.

(108) Figgis, B. N. *Introduction to Ligand Fields*; Interscience: London, 1966.

(109) Schoonheydt, R. A. *Catal. Rev.* **1993**, *35*, 129 and references therein.

(110) Texter, J.; Strome, D. H.; Herman, R. G.; Klier, K. *J. Phys. Chem.* **1977**, *81*, 333.

(111) Strome, D. H.; Klier, K. *J. Phys. Chem.* **1980**, *84*, 981.

(112) Beer, L.; Calzaferri, G.; Kamber, I. *J. Chem. Soc., Chem. Commun.* **1991**, 1489.

(113) Dědeček, J.; Wichterlová, B.; *J. Phys. Chem.* **1994**, *98*, 5721. Wichterlová, B.; Dědeček, J.; Vondrová, A. *Ibid.* **1995**, *99*, 1065. Wichterlová, B.; Dědeček, J.; Tvaruzková, Z. *Stud. Surf. Sci. Catal.* **1994**, *84*, 1555.

(114) Iwamoto, M.; Furukawa, H.; Kagawa, S. *Stud. Surf. Sci. Catal.* **1986**, *28*, 943.

(115) Anpo, M.; Nomura, T.; Shioya, Y.; Che. M.; Murphy, D.; Giamello, E. In *Proceedings of the 10th International Congress on Catalysis*; Guczi, L., Solymosi, F., Tétényi, P., Eds.; Akadémiai Kiadó: Budapest, 1993; p 2155.

(116) Chao, C.-C.; Lunsford, H. J. *J. Chem. Phys.* **1972**, *57*, 2890.

(117) Sendoda, Y.; Ono, Y, *Zeolites* **1986**, *6*, 209.

(118) Anderson, M. W.; Kevan, L. *J. Phys. Chem.* **1987**, *91*, 4174. Schlick, S.; Alonso-Amingo, M. G.; Eaton, S. S. *Ibid.* **1989**, *93*, 7906. Larsen, S. C.; Aylor, A.; Bell, A. T. *Ibid.* **1994**, *98*, 11533. Liu, S.-B.; Lin, T.-S.; Yang, T.-C.; Chen, T.-H.; Hong, E.-C.; Ryoo, R. *Ibid.* **1995**, *99*, 8277.

(119) Lei, G.-D.; Adelman, B. J.; Sárkány. J.; Sachtler, W. M. H. *Appl. Catal. B* **1995**, *5*, 245.

(120) Slovetskaya, K. I.; Alimov, M. A.; Aleshin, E. G.; Kucherov, A. V.; Slinkin, A. A. *Kinet. Katal.* **1996**, *37*, 127.

(121) Szostak, R. M. *Molecular Sieves*; Van Nostrand Reinhold: New York, 1989. Meier, W. M.; Olson, D. H. *Atlas of Zeolite Structure Types*; Butterworths: London, 1987.

(122) Redondo, A.; Hay, P. J. *J. Phys. Chem.* **1993**, *97*, 11754.

(123) Miyamoto, A.; Himei, H.; Oka, Y.; Maruya, E.; Katagiri, M.; Vetrivel, R.; Kubo, M. *Catal. Today* **1994**, *22*, 87.

(124) Zecchina, A. *J. Phys. Chem.* Manuscript in preparation.